3
Natural Nanobiocomposites, Biomimetic Nanocomposites, and Biologically Inspired Nanocomposites

Paul V. Braun

3.1
Introduction

Self-organization and directed assembly of biological macromolecules and inorganic materials plays an important role in the creation of the nanostructured and nanocomposite materials so commonly found in biology. Over the past 10 years, materials scientists and chemists have made considerable efforts to create synthetic analogs of biological materials by attempting to mimic biology and, importantly, to learn the design rules of biological systems. Considerable efforts have also been made to use what has been learned from biology to create new materials with properties not found in biological systems. All this effort has been made because natural materials unquestionably have exquisite properties not found in synthetic materials. And additionally, biological systems can produce these exquisite materials at or near room temperature in aqueous environments, whereas most synthetic schemes that produce materials often inferior to natural biomaterials require elevated temperature and pressure and harsh chemicals.

Biological nanocomposite materials can be entirely inorganic, entirely organic, or a mixture of inorganic and organic materials. Even where the final material may be entirely one class of material, multiple classes of materials may have been involved in the synthetic process, which may or may not remain in the final structure. A good example of a biological nanocomposite in which the organic material does not remain in the final product is the enamel of the mature human tooth, which is 95 % by weight hydroxyapatite. During tooth formation, enamel consists of a composite of proteins (primarily amelogenin and enamelin) and hydroxyapatite; however, the proteins are removed as the tooth develops. The presence of the proteins, and the self-assembled structures they form with other biological macromolecules, do however help generate the mineral cross-ply structure of the enamel, which plays a large part in its observed toughness. The best known example of an inorganic/organic structural composite for which both phases remain in the final product is the aragonitic nacreous layer of the abalone shell, which is exceptionally strong because of its organic/inorganic layered nanocomposite structure, in which crystalline ceramic layers are sepa-

Nanocomposite Science and Technology. Edited by P.M. Ajayan, L.S. Schadler, P.V. Braun

ISBN: 3-527-30359-6

rated by highly elastic organic layers. However, there is much more to the exceptional properties of the abalone shell than simply its layered structure, as many researchers are discovering. Synthetic efforts have been made for about 10 years to create such a structure in the laboratory, and although some synthetic structures resemble the abalone shell, to date their properties have been inferior. Thus the practical value of the synthetic structures is limited. With the many exciting scientific discoveries that have been made, there is great potential for new materials in the not too distant future.

Many more examples of attempts to copy biology have not been as successful in generating engineering materials as one would have hoped. In hindsight, this is not surprising. Biological materials generally form over a period of days to years, use a limited set of elements, and are designed to be used within a limited temperature range. Practical engineering materials must be made rapidly (hours or minutes) and generally must operate over a wide range of temperature and other environmental conditions. The disconnect between the needs of engineering materials and of biological materials has led many scientists to conclude that, rather than attempting to directly copy biology, a much better philosophy is to learn from biology and use this knowledge to create synthetic materials. This may or may not involve the use of some biological molecules, but no attempt is made to 'copy' specific biological processes.

This chapter covers natural nanobiocomposites, biomimetic nanocomposites, and biologically inspired synthetic nanocomposites. Natural nanobiocomposites are exactly what the name implies, that is, natural composite materials with structure on the nanoscale; biomimetic nanocomposites are synthetic nanocomposite materials formed through processes that mimic biology as closely as possible; and biologically inspired nanocomposites are composite materials with nanoscale order created through processes that are inspired by a biological process or a biological material, but without attempting to mimic, or directly copy, the mechanism of formation of the biological material. There are many areas I do not attempt to cover, including mixtures of two or more materials in which the materials form a homogeneous mixture (and thus are not composites) or in which the organic molecule is simply dispersed in an organic host, such as organic molecules in a sol–gel matrix. I also only minimally cover the widely publicized work on mesoporous silica and related materials, because several very good reviews on this subject already exist [1–5].

The formation of solids containing defined nanometer-scale structures and features is a challenging goal of great interest in the synthesis of novel materials. Significant efforts have been made to generate nanostructured materials by techniques ranging from scanning microscopy to molecular self assembly [6–14]. Through careful control of molecular architecture, self-assembly can yield many different nanostructured organics. The potential for creating new materials by mineralizing, polymerizing, or otherwise replicating these organized structures is very interesting. For example, mineral growth within and on lipid aggregates has resulted in unusual morphologies, including mineralized tubules and disks [15, 16]. Another approach to controlling mineral growth through self-assembly involves the coassembly of molecular species and mineral-phase precursors into mesoporous structures. This methodology has been successful in the now widely studied formation of mesoporous oxides [17–23].

3.2
Natural Nanocomposite Materials

In biology, examples abound of structures with nanoscale dimensions, and virtually all the functionality provided by these materials is a direct consequence of the nanoscale dimensions of the structure. A few examples of nanoscale materials in biology are lipid cellular membranes, ion channels, proteins, DNA, actin, spider silk, and so forth. In all these structures, the characteristic dimension, at least in 1D, and often in 3D, is on the order of a few nanometers. Although a materials scientist does not typically consider such materials to be composites, in truth, the properties of many biological materials are driven by structure on the nanoscale and, in the sense that the larger material is composed of discrete nanoscale building blocks, most of these biological materials can be considered nanocomposite materials. In their active form, that is, when folded, proteins are composed of domains with varying hydrophilic and hydrophilicity, as well as domains with such structural features as alpha helixes, beta sheets, and turns. The assembly of proteins into these complex structures containing nanometer-sized domains of varying chemical properties gives proteins, as well as many other biomolecules, their intriguing properties. Because these chemically diverse regions can exhibit acidic, basic, hydrogen-bonding, hydrophilic, or hydrophobic behavior, they can interact in exceedingly diverse ways with precursors for mineral compounds and the final mineral product. The inorganic/organic composite materials formed by these exceedingly complex biomolecular structures are the primary focus of the rest of this section.

However, before discussing inorganic/organic nanocomposites, a short discussion of at least one completely organic nanocomposite with outstanding properties, namely spider silk, is in order. Dragline spider silk, which makes up the spokes of a spider web, is five times tougher than steel by weight and can stretch 30%–40% without breaking. However, to be fair to steel, I should point out that, although the work-to-failure is greater for silk than steel, the elastic modulus of silk is significantly less than that of steel. For applications in which flexibility and toughness are the primary need, a synthetic route to creating a material with properties equivalent to spider silk would be exceedingly valuable. The strong core of spider silk is composed primarily of two protein components that self-assemble into crystalline and amorphous regions. The crystalline regions consist of alternating alanine-rich crystalline forming blocks, which impart hardness [24–26], and glycine-rich amorphous blocks, which are believed to provide elasticity [27]. This nanocomposite structure of organic nanocrystals in an amorphous organic matrix generates the exceptional properties of spider silk. Spiders cannot be kept in close quarters and harvested, because they eat one another; thus the only route to creating quantities of spider silk sufficient for application will be synthetic.

Knowledge of the molecular structure of spider silk is not sufficient for creating a synthetic material with its properties. Inside the spider, the silk precursor exists as a lyotropic liquid crystal that is approximately 50% silk. As the silk is excreted, the protein molecules that make up silk fold and are aligned as they approach and then pass through the spinneret, forming a complex insoluble nanostructured fiber. In fact, not

only is the spider silk made up of crystalline and amorphous regions, but the crystalline regions are in turn composed of both highly oriented crystals and less oriented, but still crystalline, regions [28, 29]. These poorly oriented crystalline regions may serve to mechanically couple the highly oriented crystalline structure with the amorphous domains. This three-phase morphology presumably has properties exceeding those of a similar two-phase system because of better coupling between the phases, due to the smaller mismatch in mechanical properties at the interface between the various domains.

Recently, a synthetic spider silk-like material with properties approaching those of natural spider silk has been created. Because of their high complexity, the silk precursors could not be created by conventional organic synthesis and thus were created by expressing two of the dragline silk genes in mammalian cells [30]. The resulting soluble recombinant dragline silk proteins were wet-spun into fibers of diameters ranging from 10 to 40 micrometers. After a postspinning draw, fibers with mechanical properties approaching those of natural spider silk were obtained. The fibers were highly birefringent, indicating a high degree of chain orientation, but it is not yet known if the internal nanostructure of the fibers was similar to that of natural spider silk. Work is now ongoing to build up a herd of transgenic goats that express spider silk proteins and excrete them in their milk, which should result in the production of sufficient silk protein for manufacturing.

Much like the nanostructure of natural silk, which self-organizes in the biological organism, natural organic/inorganic nanocomposites are also formed through self-assembly. The two extremes of the mechanism for formation of natural nanocomposites are when the organic matrix forms first, followed by mineralization, and when the organic and inorganic materials coassemble into the nanostructured composite. There do not appear to be any examples in which the inorganic structure forms first, followed by organic structure formation. Most biological composites appear to form through the first route; a process whereby an organic structure first forms, followed by the biologically directed nucleation and growth of a mineral phase. However, it is also clear that the organic matrix restructures and reorganizes continuously as the mineral deposits, which resembles the second mechanism. With both mechanisms, the organic material is generally composed of an amazing diversity of macromolecules, including proteins and other biopolymers. Considerable effort has been made to understand the mechanism of formation of these composite materials, a process that requires an understanding of both the structure and function of the organic matrix and the interactions between the organic matrix and the inorganic precursors and product.

The simplest examples of biological nanocomposites are those in which the mineral phase is simply deposited onto or within an organic structure. The next level of complexity is shown by examples in which the structure of the mineral phase is clearly determined by the organic matrix. The greatest complexity is where the mineral is intimately associated with the organic phase to create a structure with properties that are superior to those of either the mineral or organic phase. In the first and second examples, the organic phase forms first, but in the third, the organic and inorganic phases almost certainly coassemble into the final structure.

3.2.1
Biologically Synthesized Nanoparticles

For the simplest example of a biological nanocomposite, one needs to look no farther than the grasses. Many species of grass precipitate SiO_2 nanoparticles within their cellular structures. Perhaps due to some internal structure in their cells, the silica nanoparticles generated within the cells can be found in sheet-like, globular, or rod-like morphologies, with characteristic dimensions ranging from a few nanometers to tens of nanometers (Figure 3.1**)** [31]. The exact reason for the silica deposition is not known, although it may simply be a way for the plant to sequester silica, which it continuously takes in as dissolved silicic acid and other silica-containing soluble species. If the plant could not sequester silica, it would build up and potentially limit growth. At high levels, silica may make the plant undesirable as food [32], for example, the dry weight of horsetails consists of 20 % – 25 % silica.

Another example of a biologically simple organism that can generate internal nanocomposite structures is bacteria, the most famous of which are magnetic bacteria, which contain an internal chain of magnetite (Fe_3O_4) nanocrystals running down their long axis (Figure 3.2). These nanocrystals are about 40 nm in diameter and give the bacteria a net magnetic moment, which aligns them with respect to the earth's magnetic field. The presence of this magnetic chain of nanocrystals plays a role in defining

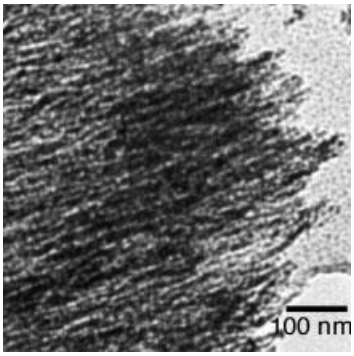

Fig. 3.1 Transmission electron micrograph of rod-like amorphous silica extracted from a grass. The rod-like nature is due at least in part to the local environment inside the plant cells. Adapted from [31]

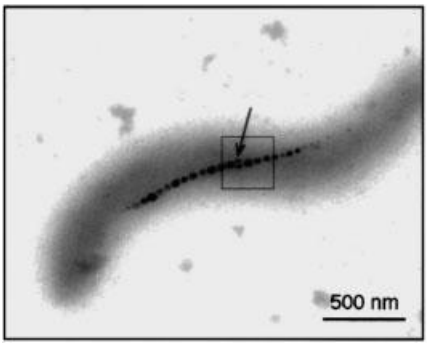

Fig. 3.2 Transmission electron microscope bright-field image of a single cell of *Magnetospirillum magnetotacticum* strain MS-1. Off-axis electron holography of the boxed region in the transmission electron microscope showed that the magnetite crystals were all single magnetic domains. Adapted from [161]

the direction of locomotion. Because an individual bacterium, on average, points in a specific direction, as it moves it continuously explores fresh territory. In contrast, the movement of a bacterium lacking a directing force follows a random walk, resulting in a substantially lower probability for movement into fresh territory. Besides the Fe_3O_4-containing bacteria, other bacteria deposit chains of nanoparticles of the magnetic mineral greigite (Fe_3S_4) within themselves. This mineral chain appears to serve the same function as the Fe_3O_4 chain in the previous bacteria.

3.2.2 Biologically Synthesized Nanostructures

Biological organisms commonly synthesize nanostructured and nanocomposite materials of much greater complexity than nanoparticles. These structures can come in many forms, ranging from needles and plates to complex 3D nanostructures, and can exhibit many unique and interesting mechanical, chemical, and optical properties. Although simplifying all biological nanostructure formation routes into a single mechanism is not possible, several general synthetic tenets tend to hold true. The first is that the biological structure forms first, and then the inorganic phase begins to form. Although truly cooperative assembly is possible, it is much more common that the organic matrix forms first, regulating the growth of the inorganic material. We should keep in mind, however, that the organic matrix is plastic and can deform or reshape in response to the growing inorganic material.

Besides forming nanoparticles, bacteria can form more complex nanostructures. Bacteria in general are responsible for a vast amount of mineral deposition and in fact can contribute greatly to mineral deposits on the bottoms of lakes and other aquatic environments. Mineral formation in the vicinity of bacteria is generally driven by a biologically induced change in the pH or ionic strength around individual bacteria. This change in the local environment reduces the solubility of certain mineral compounds, leading to precipitation of minerals. Generally, this results in an unfeatured mineral, so is not of interest here. However, in specific cases, the structure of the precipitated mineral is highly regulated by proteins on the surface of the bacteria, resulting in the formation of complex nanostructures. Specifically, some bacteria have on their exterior a layer of proteins called an S-layer. As these bacteria respire, the local pH and ionic strength change, driving, for example, the mineralization of gypsum ($CaSO_4$). Rather than being deposited as an unfeatured solid on the exterior of the bacteria, the growing gypsum is templated by the organic S-layer into a complex nanostructured form that very closely replicates the structure of the protein S-layer (Figure 3.3) [33, 34]. The exact mechanism of the mineral templating is not known, but clearly preferred sites must exist on the S-layer for heterogeneous nucleation of mineral, or a regular structure would not form. As these mineral nuclei grow, they impinge on one another, forming a thin, periodically structured film of gypsum. One reason for the complexity of this structure is that the resulting pores in the inorganic layer may allow the bacterium to exchange nutrients with its surroundings even after the mineral phase forms. If the gypsum had formed as a dense solid film, it would rapidly stop the bacterium's respiration, thus killing it.

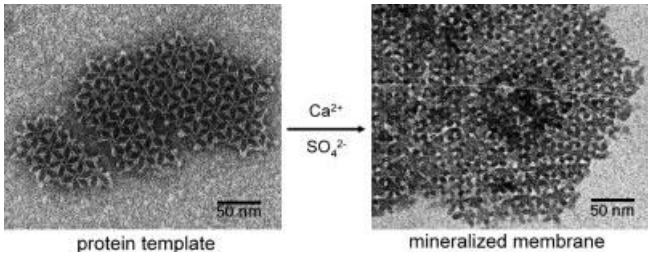

Fig. 3.3 Transmission electron micrograph of (left) bacterial S-layer, which serves as a protein template for the formation of (right) a thin film of mesostructured gypsum. Adapted from [33]

Although this specific S-layer templated structure as yet has no known applications, inorganic nanostructures of these length scales are of great interest for many high-technology applications. Patterning on these length scales is exceedingly difficult, so if bacteria could be genetically engineered to express proteins that result in S-layers having technologically significant nanostructures, there would be the potential to biomineralize materials for advanced applications. In fact, initial strides have been made in this regard and are covered later in this chapter.

Higher organisms also generate inorganic/organic composite structures. An excellent example is the sea urchin. The sea urchin spine is a single crystal essentially composed of calcite, containing only about 0.02 % glycoproteins trapped within the crystal lattice of the spine [35]. However, this very small amount of organic matter leads to the extraordinarily high toughness and unique fracture properties of the spine. The spine is much tougher than a synthetic equivalent composed of polycrystalline or single-crystalline calcite. Most surprising is the fracture mode of the spine. Rather than fracturing along a specific crystallographic direction, as occurs for most single crystals, it fractures with conchoidal cleavage, that is, with a smooth rounded fracture surface, similar to that observed for glassy materials (Figure 3.4). The fact that it is a single crystal but does not fracture along any specific crystallographic direction is quite unlike almost all other crystalline ceramic materials. The mechanism for the toughening is still unknown but is clearly due at least in part to the nanoscale dispersion of protein molecules in the crystal lattice.

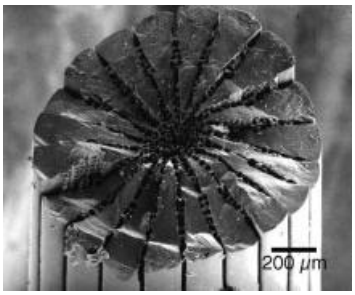

Fig. 3.4 Scanning electron micrograph of the fracture surface of a single-crystal spine from a sea urchin, demonstrating conchoidal cleavage. Adapted from [35]

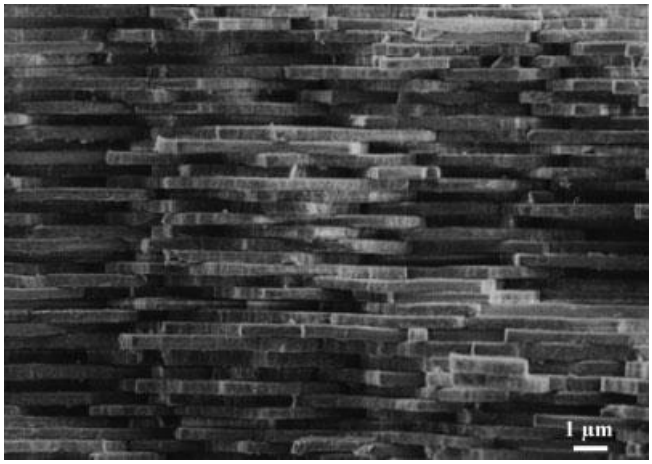

Fig. 3.5 Scanning electron micrograph of a fracture surface of the nacre of the red abalone, showing a side view of the aragonite tablets. Adapted from [162]

Another sea creature that creates an organic/inorganic composite that is vital to the creature's survival is the abalone, as already mentioned. The nacreous (mother-of-pearl) layer of the abalone shell consists of alternating layers of 500-nm-thick aragonite platelets and ~30-nm-thick sheets of an organic matrix **(**Figure 3.5**)**. The matrix forms first, then the mineral plates develop between the layers. The matrix defines the thickness of the crystals, and certainly also adds to the strength of the composite structure by forcing fractures to dissipate their energy as they travel a tortuous path through this elastic structure. The matrix also controls the crystallographic orientation of the mineral plates, which must also be important for strength. The resulting composite structure has a fracture toughness that is about 3000 times greater than that of inorganic aragonite [32]. Along with defining the size and shape of the aragonite plates, the organic matrix also likely serves to define their crystallographic orientation. The mechanism for formation of nacreous aragonite is not entirely clear, although it is known that the organic matrix forms first into a hollow layered structure, and then the voids in this structure are mineralized.

Another excellent example of a biological nanocomposite with complex structure and function is bone. Bone must perform multiple functions. It must have high strength, yet low weight; it must support remodeling in response to applied stresses, yet not deform under applied stress; it must contain pores to allow oxygen and nutrients to reach the cells within the bone, yet these same pores cannot lead to fractures; finally, it must act as a reservoir for minerals, but not allow itself to demineralize and thus weaken. Bone exists in several forms; lamellar bone provides the structural properties of long bones in mammals and other species and is the subject of the following discussion, adapted from [36, 37] (Figure 3.6). The basic structure of bone is a mineralized collagen fibril consisting of on average 65 % mineral, the remainder being organic material and water. The collagen phase of bone is composed of individual fibrils about 80 – 100 nm in diameter. These fibrils are in turn composed

of assemblies of a triple helix of polypeptide chains with an average diameter of 1.5 nm and length around 300 nm. The internal arrangement of this triple helix structure in the collagen fibril is not random: the helix aligns with its long axis parallel to the long axis of the bone and has additional fine structure. The mineral phase of the bone,

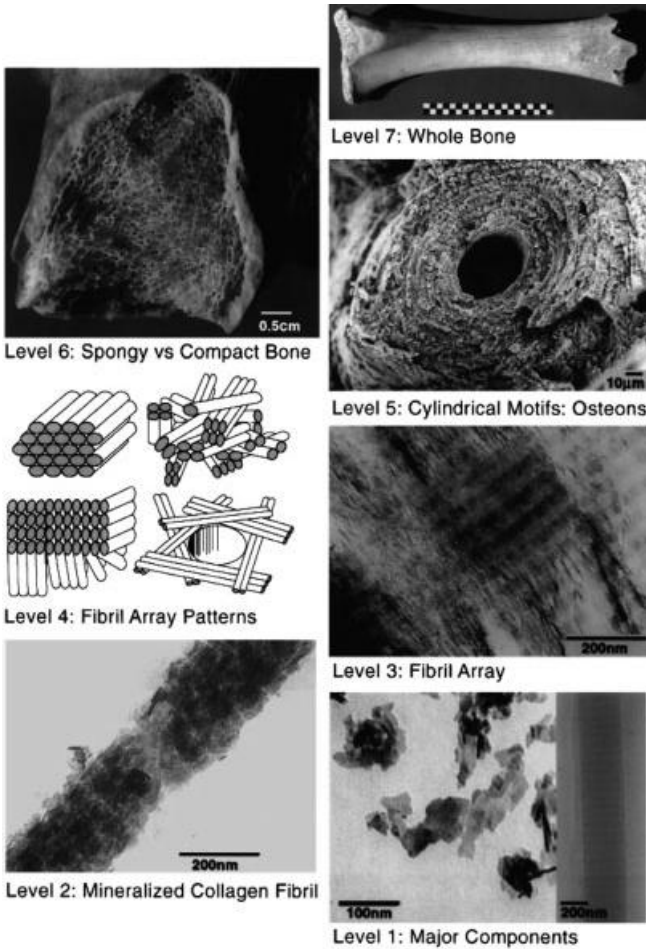

Fig. 3.6 The 7 hierarchical levels of organization of the bone family of materials, according to Weiner [37]. Level 1: Transmission electron micrographs of individual mineral crystals from human bone (left side) and an unmineralized, unstained collagen fibril from turkey tendon embedded in vitreous ice (right side). Level 2: Transmission electron micrograph of a mineralized collagen fibril from turkey tendon. Level 3: Transmission electron micrograph of a thin section of mineralized turkey tendon composed of multiple fibrils. Level 4: Four fibril packing motifs found in the bone. Level 5: Scanning electron micrograph of a single osteon from human bone. Level 6: Light micrograph of a fractured section through a 5500 year old fossilized human femur. Level 7: Whole bovine bone (scale: 10 cm). Adapted from [37]

carbonated apatite ($Ca_5(PO_4,CO_3)_3(OH)$), forms as 50-nm-long, 25-nm-wide platelets that are on average 1.5 – 4 nm thick (Figure 3.7). These platelets lie within the collagen fibrils, with only a small number of polypeptide chains between each platelet. The long axis of the platelets is generally parallel to the outer surface of the bone, most likely to maximize the compressive strength of the bone.

The mineral structure forms in bone after the collagen fibrils form. However, as the mineral forms, the collagen structure may reorganize to some extent. Thermodynamically, the carbonated apatite platelets should coarsen into larger single crystals over time (Ostwald ripening), but clearly this is prevented by the collagen matrix. Thus, although the collagen matrix reorganizes to some extent, it clearly cannot be completely pushed out of the way by the growing mineral. This level of control by biology over structural development during mineralization currently exceeds that found in synthetic materials. Additionally, after a bone is broken, new structures form which generate material that is as strong as the original bone; yet, the mineralization process stops when the healing process is complete. Bone thus is an excellent example of a self-healing biological nanocomposite in which an organic host phase is formed, followed by highly regulated mineralization processes. The mechanism for this process is not entirely clear, but substantial strides in understanding it are being made.

Clearly, biological systems can create a tremendous diversity of inorganic materials; however, biological systems are also very limited in terms of material selection. Metals, as well as many polymers, semiconductors, and ceramics cannot be synthesized by biological processes, because the precursors are not available in the natural environment, the materials or precursors are toxic, and/or the product is not stable in the

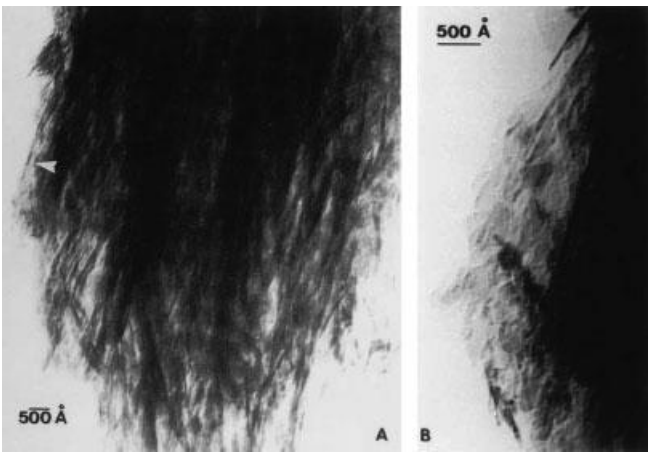

Fig. 3.7 Transmission electron micrograph of a fractured piece of mineralized bone from a 50-year-old human male femur. (a) Many mineral crystals are oriented edge-on and are parallel to the long direction of the collagen fibrils. (b) Higher magnification view of the bone fragment at the location in (a) marked with an arrowhead. Here, crystals are oriented face-on. The flat, plate-like nature of the mineral crystals in bone can be observed in these figures. Adapted from [163]

presence of water and/or oxygen. Because of this, there is serious interest in using elements of biological systems to create synthetic nanocomposites from materials not found in biology, thus achieving the best of both the biological and synthetic worlds.

3.3
Biologically Derived Synthetic Nanocomposites

Because of the limited variety of materials available by purely biological routes, there is great interest in utilizing the sophistication offered by biological systems in concert with synthetic procedures to create materials with otherwise unobtainable nanostructures and thus, potentially, unique properties. Biology offers a unique selection of building blocks that would be difficult or impossible to synthesize in the laboratory. These include proteins, DNA, RNA, and small but highly functional molecules.

3.3.1
Protein-Based Nanostructure Formation

As already mentioned, protein S-layers on the surface of bacteria create complex nanostructures. The protein S-layer present on the surface of some bacteria has now also been used to create entirely synthetic nanostructures. The diversity of S-layer structures, coupled with the potential for chemical functionalization, make them ideal starting points for nanostructure synthesis. To review, S-layers are 2D protein crystals that have oblique, square, or hexagonal lattice symmetry with lattice constants between 3 and 30 nm. Interesting for potential nanostructure formation, and to enable bacterial respiration, S-layers almost universally contain pores of identical size and identical surface chemistry – properties that make S-layers useful for nanostructure and nanocomposite fabrication. In an early example [38, 39], an S-layer was used to template a periodic structure into a thin metal film. Specifically, a 1-nm-thick metal (Ta/W) film containing 15-nm holes periodically arranged in a triangular lattice with a lattice constant of 22 nm was created by S-layer templating. This was accomplished by first depositing a suspension of S-layer fragments onto an amorphous carbon support film. After S-layer deposition, a 1.2-nm thick film of Ta/W was evaporated onto the S-layer at an angle of 40° from the normal of the substrate surface. When examined in the transmission electron microscope (TEM), the resulting film shows contrast indicating some thickness variation in the metal, but the contrast is not significant. To improve the contrast and to open up holes in the metal film, the film was argon-ion-milled for a short time. The result was a metal film that contained a periodic array of holes with the same symmetry as in the S-layer template [38, 39]. This work was done more than 15 years ago, yet creating such a nanostructure today would still be a challenge, even with a modern e-beam lithography system.

Much more recently [13], an S-layer was used to create nanostructured semiconductor films. The S-layer in this study had an oblique 2D lattice (space group p_1; a = 9.8

nm, $b = 7.5$ nm, $\theta = 80^\circ$). Depending on the mechanism of S-layer deposition, either its negatively charged inner face or its charge-neutral outer face was exposed to a 10 mM $CdCl_2$ solution. After drying, the cadmium-ion-doped S-layer was exposed to H_2S gas, resulting in formation of a nanocrystalline film of the semiconductor CdS on the S-layer. In the TEM, the CdS film exhibited a superlattice structure that was a direct copy of the structure of the S-layer [13]. The S-layer may have survived the entire process, and thus the actual mineral structure formed may be a nanocomposite of CdS and protein. It is still unclear what applications might be found for such materials, although robust metal or semiconductor nanoporous structures may find application as filter membranes, sensors, and optoelectronic devices.

Another protein assembly that has been used to form nanocomposite materials is ferritin (Figure 3.8**)**. In its native form, ferritin consists of a supramolecular arrangement of proteins around an iron oxide core. The iron oxide core can be selectively dissolved without damaging the structure of the protein shell, yielding a hollow ball of protein about 10 nm in diameter. The demineralized protein (apoferritin) can be refilled with iron oxide, demonstrating that its structure was not greatly affected by the demineralization process. Interestingly, apoferritin can also be filled with other mineral nanoparticles. In one example [32], the iron oxide core of ferritin was converted to FeS by treating the ferritin with H_2S. Nanoparticles of MnOOH, UO_3, Fe_3O_4, and CdS can also be formed inside apoferritin through the appropriate chemi-

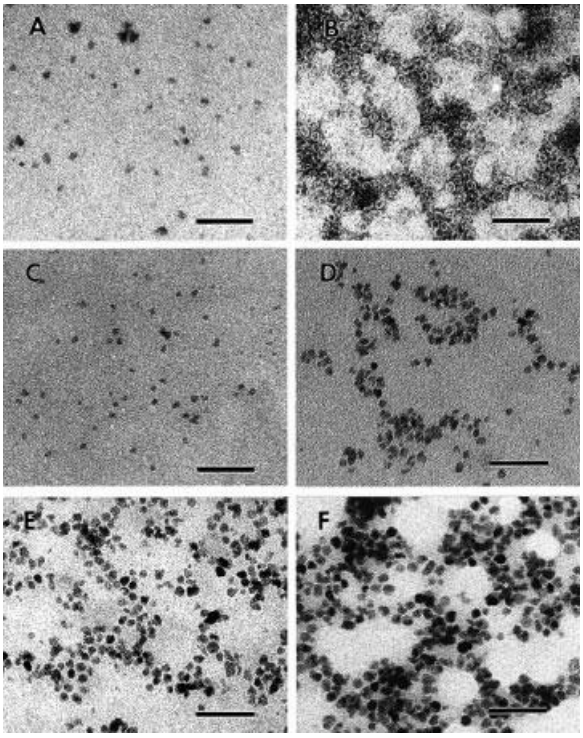

Fig. 3.8 Transmission electron micrographs of magnetite (Fe_3O_4)- and maghemite (γ-Fe_2O_3)-filled ferritins. (a) 260 Fe atoms/molecule, unstained; only the discrete electron-dense inorganic cores can be seen. (b) 260 Fe atoms/molecule, after staining with uranyl acetate, showing encapsulation of inorganic cores by intact protein shell (white halo around each particle). (c) 530 Fe atoms/molecule, unstained. (d) 1000 Fe atoms/molecule, unstained. (e) 2040 Fe atoms/molecule, unstained. (f) 3150 Fe atoms/molecule, unstained. Scale bars in all figures = 50 nm. Adapted from [164]

cal treatment. Because the protein shell is not disrupted by the mineralization process, the final product is truly a nanocomposite of protein and inorganic material. See [32] for an extended discussion of the use of apoferritin as a template for synthesizing nanocomposite materials.

3.3.2 DNA-Templated Nanostructure Formation

DNA offers great potential as a building block for nanocomposite materials. It can be tethered to a wide range of substrates, can direct assembly with specificities that greatly exceed that of any synthetic molecule, is relatively robust, can be synthesized in relatively large quantities, and can be functionalized with tags such as fluorescent molecules to enable rapid detection of binding events.

The use of DNA to assemble and create nanostructures and nanocomposite materials is only in its infancy, but even the preliminary work done so far indicates the great potential of DNA-based assembly techniques. A few of the approaches that have been studied to date include the mineralization of DNA, the use of DNA to assemble nanoparticles, and the use of DNA to assemble much larger colloidal particles. These three approaches are outlined in this chapter; however, the number of possibilities is vast, and significant work on DNA-mediated assembly of nanostructures is currently being done.

The possibility of using plasmid DNA as a template for mineralization was first explored in 1996 [40]. In this work, single strands of a 3455-basepair circular plasmid DNA were mineralized with CdS nanoparticles, by mixing the plasmid and cadmium perchlorate in solution, followed by spin coating this solution onto a polylysine-coated glass slide. The DNA/cadmium perchlorate-coated glass slide was then exposed to H_2S, converting the cadmium perchlorate to CdS, which preferentially mineralized the DNA. This procedure results in ring-like structures consisting of DNA embedded within a 5–10-nm-thick CdS strand that can be directly observed in the TEM (Figure 3.9). The diameter of the ring formed by the CdS-encrusted DNA is directly related to the diameter of the DNA plasmid, and the thickness of the CdS/DNA composite strand is about 10 nm. This represents the first example of DNA templating of semi-

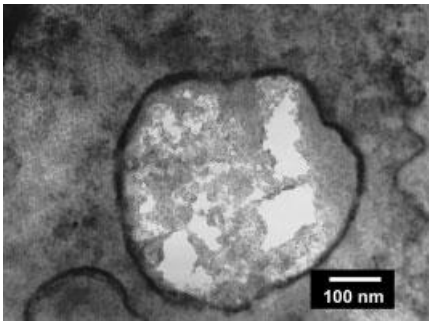

Fig. 3.9 Transmission electron micrograph of a nanostructure obtained by mineralization of a circular plasmid DNA with CdS nanoparticles. The ring diameter closely matches the predicted diameter of the plasmid DNA. Adapted from [40]

conductors but, given the vast array of structures that can be formed from DNA, should not be the last.

Another example of DNA-based nanostructure development can be seen in the work on DNA-based nanoparticle assembly. Several approaches have been explored, with the majority based on the Watson–Crick base-pairing of DNA strands attached to various nanoparticles. The first approach involved the functionalization of gold nanoparticles with multiple strands of thiol-terminated type-A or -C DNA in separate reactions [41] (where 'type' is used as a label for different nucleotide sequences). The thiol terminal group is important, because it enables covalent attachment of the DNA strand to the gold nanoparticles. Importantly, the A and C strands were designed so that they would not hybridize. The result, after mixing the solutions of each kind of DNA-functionalized nanoparticles, is a simple mixture of DNA-functionalized gold of type A and DNA-functionalized gold of type C. Then a single strand of DNA with one end complimentary to the type-A DNA and the other end complimentary to the type-C DNA was added. We label this strand B-D. Upon hybridization of the B-D strand with both nanoparticles of type A and nanoparticles of type C, a DNA-linked aggregate of nanoparticles was formed. Aggregate formation is thermally reversible by increasing the temperature above the melting point of the DNA, at which point the strands dehybridize. The assembly could be monitored by UV/visible spectroscopy, because the UV/visible absorption of gold nanoparticles changes greatly when they are close together, due to changes in the surface plasmon.

The formation of controlled aggregates, although interesting, is really a starting point for the creation of much more complex structure through a marriage of biological macromolecules and synthetic materials. In addition to placing multiple DNA molecules on a nanoparticle, it is possible to place a single or a finite number of DNA molecules on a nanoparticle. However, this requires a significant degree of synthetic effort, because one usually starts with a population of nanoparticles with various numbers of attached DNA molecules. Through careful separation, nanoparticles with exactly one or exactly two single-stranded DNA molecules on their surface can be recovered. These DNA-functionalized particles can then be assembled in highly controlled fashions through DNA hybridization reactions, by adding single-stranded DNA that is complimentary to the single-stranded DNA on the nanoparticles **(**Figure 3.10**)**. This is similar to the approach used to make DNA-linked aggregates; however, because each nanoparticle contains only one DNA strand, not multiple strands, the result after hybridization is not the formation of an aggregated structure, but rather, individual dimers of gold nanoparticles. Trimers of gold nanoparticles were also created by a similar approach, except that nanoparticles with one strand of DNA of three different sequences was mixed with a strand of DNA complimentary to all three of the DNA strands on the surface of the nanoparticles [42, 43].

Recently, it was demonstrated that DNA can assemble much larger colloidal particles into 3D assemblies of controlled shape. The basic approach is very similar to the assembly of nanoparticles; however, here the results after hybridization are assemblies of colloidal particles with defined connectivity [44].

The overall power of DNA-based assembly of nanostructures is based on several powerful aspects of DNA hybridization. First, hybridization is reversible with tempera-

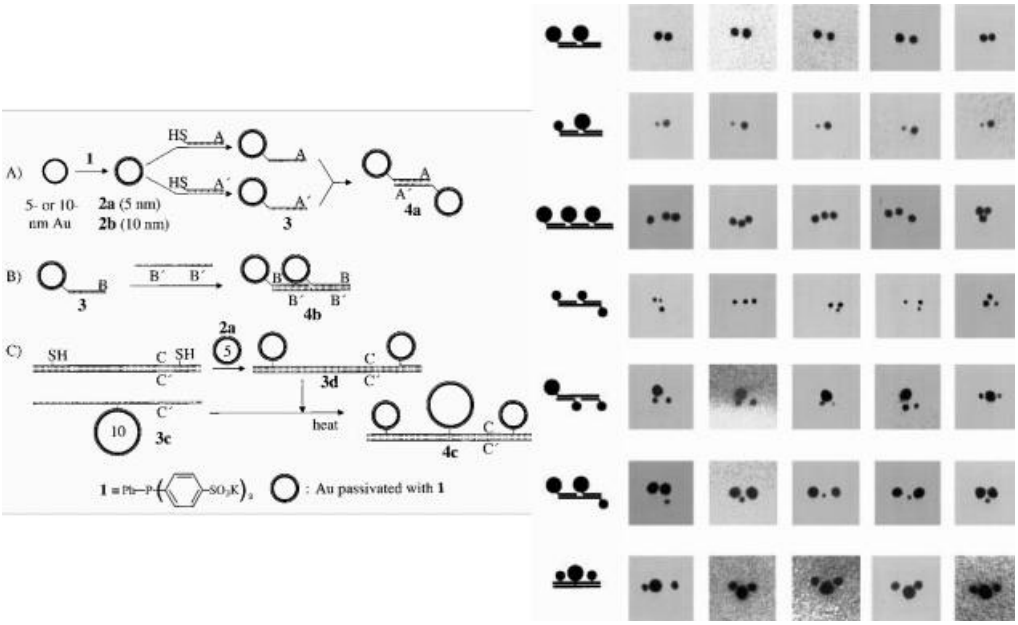

Fig. 3.10 DNA allows for precise manipulation of the order and spatial arrangement of nanoparticles. The large and small nanoparticles can be designed to hybridize or react with a single site on the DNA backbone. See examples A, B, and C on the left and the resulting nanostructures on the right. Adapted from [43]

ture; thus it is possible to anneal structures that at least partially eliminate kinetic traps that may be present in the assembly process. For example, if during nanostructure assembly, a particle does not hybridize in the correct location, the structure can be gently heated, releasing the particle, and then the particle can be retrapped by cooling below the melting point of the DNA. Second, DNA hybridization is very specific. Unlike most organic linking chemistries, which cannot distinguish small changes in molecular structure, DNA can be designed to hybridize only to its exact complimentary strand. Thus it may be possible to combine many DNA-functionalized nanoparticles into very specific arrays by hybridizing to a long strand of DNA that is encoded so as to react with each DNA functionalized nanoparticle at only a very specific location.

3.3.3 Protein Assembly

To achieve a level of complexity similar to what can be obtained by DNA-based assembly, one can engineer or select biological organisms that recognize and bind with high specificity to specific minerals, semiconductors, and metals. In the first example [45], *Escherichia coli* containing genetic sequences specific for recognizing and binding iron oxide but not other metal surfaces was identified and multiplied. Bacteria that would

specifically adhere to iron oxide were identified via serial enrichment from a population of bacteria. The experimental procedure was as follows: A population of genetically diverse *E. coli* was exposed to iron oxide particles. The bacteria that bound to the iron oxide were collected, and the remainder were discarded. After repeating this procedure for several generations, bacteria with high degrees of specificity for iron oxide were obtained. The reason only some of the bacteria bind iron oxide is that *E. coli*, like many other bacteria, express proteins on their outer surface whose sequences are a function of the unique genetic makeup of the bacteria. By starting with a library of $\sim 10^7$ *E. coli* that express surface proteins of slightly different sequences, the probability that at least one of the *E. coli* has a highly specific protein is reasonable. Through enrichment, it is possible to extract and multiply just those bacteria that bind to the surface of interest.

It is also possible to select for protein sequences that attach to specific metal surfaces, and presumably also to metal nanoparticles. Through such biological experiments, a library of $\sim 10^7$ different polypeptides 14 or 28 amino acids long was created. Then, the polypeptides that adhere to the metal surface were isolated, and their sequences were determined [46]. This approach is exceedingly powerful because of the vast number of different molecular sequences that can be studied in parallel in a single experiment.

From a technological standpoint, it is interesting to consider the possibility of recognizing semiconductor surfaces and semiconductor nanoparticles with this procedure. If an appropriate genetic sequence can be identified, it would be possible to assemble nanoparticles via biological organisms that are designed to present the appropriate biological macromolecules on their surface. Phage display enables the simultaneous testing of many peptide sequences for specificity to a given surface. A phage library containing 10^9 polypeptide sequences was exposed to a surface, and all the phages that did not bind to the surface were washed away. The phages that stuck were then removed from the surface by lowering the pH and were amplified by infecting *E. coli* bacteria with them. This process was repeated until only phages that stuck strongly to the surface were present. The DNA of these phages was then sequenced to determine the specific peptide sequence(s) that bind with such high affinities to the specific surface of interest [47].

A phage that identifies and binds to a surface of a specific material also binds strongly to nanoparticles of this material. The result of mixing a nanoparticle-binding phage with nanoparticles is 'decoration' of the phage with nanoparticles, which occurs only at the end of the phage that contains the specific binding polypeptide, and nowhere else on the phage [48]. Depending on the experimental conditions and phage design, it may even be possible to bind single nanoparticles to an individual phage or to assemble the nanoparticles into defined structures, although in the present state of the art, multiple nanoparticle are bound in a fairly random fashion to each phage.

3.4 Biologically Inspired Nanocomposites

The properties of biocomposites and synthetic pathways for their formation have inspired wide ranging research. However, early on it was recognized that it is not always necessary or even desirable to use biologically derived materials for many applications and that it may be possible simply to use biology as an inspiration for totally synthetic nanocomposite systems. It is interesting to consider biological systems as an inspiration for nanocomposite materials, because biological systems exhibit many characteristics that would be attractive in synthetic materials, but it is also clear that direct mimicking of biology will be limited to a specific small subset of materials and to specific nanostructures. However, many lessons can be learned from biology on how to form complicated nanostructures and on the potential properties of these synthetic nanostructured materials, should one be successful in synthesizing them. Of course, just because a synthetic material resembles a natural process and the process of forming that material resembles a natural synthesis does not always mean that the scientists and engineers who performed the work were inspired by biology. Often it is not stated whether biology was an inspiration for the work, and thus some care must be taken before assuming that, just because something appears biologically inspired, it is biologically inspired. In this chapter, I do not attempt to make this distinction and by necessity assume that, if the work has a biological analog, then it can be considered 'biologically inspired', although certainly in some cases this assumption may be wrong. In this chapter I take the liberty to lump such work under the heading of 'Biologically Inspired Nanocomposites'.

Much can be learned from biological systems to further the development of synthetic approaches to the formation of complex inorganic structures. Each of the routes to nanostructure formation that is discussed in this section – liquid crystal templating, colloidal particle templating, block copolymer templating, and surfactant-inorganic self-assembly (mesoporous silica being the most famous of this approach to nanostructure formation) – invokes many of the tenets of biologically directed mineral growth. As already discussed, biological systems rely on self assembly and mineralization in the synthesis of hard inorganic structures such as shells, teeth, and bone [11], and their approaches to materials fabrication can provide guidance and direction to synthetic systems. Often, the term 'biomimetic' has been applied to any approach using self assembly in the synthesis of nanocomposite materials. As mentioned above, biological systems do indeed use self-assembling molecules, and high levels of molecular organization are a very important part of an organism's inorganic structure development. However, it would be naive to expect to simulate this process in the laboratory except on the most basic level. Biological processes are extremely dynamic, involving huge numbers of very specific proteins and other molecules being generated and transported to very specific locations, with temporal control. The best synthetic systems are indeed very simple approximations of living systems and generally are much too simple to be considered to be truly mimicking biology. Although the synthetic systems are only simple approximations of life, still much can be learned by attempting to mimic living systems [8], even if biomimetic is perhaps not the best

term. For example, many attempts centered around the synthesis of mineral phases in a self-organized matrix have indeed mimicked the mineralization processes of many biological systems. Examples of matrix-mediated biological mineralization processes include the reliance of bacteria, plants, shells, and even mammals on organically mediated growth of mineral phases to eliminate byproducts (bacteria and plants) [31, 33, 34], create exoskeletons (shells) [49], and grow teeth (mammals) [35]. If during the synthetic process, organic molecules are incorporated into the mineral phase, the resulting material may resemble the spicule of a sea urchin, which contains much less than 1% protein intercalated into the crystal lattice [35].

Despite the low degree of sophistication of synthetic systems, they do have very distinct advantages over biologically based schemes. Biological systems operate with only a limited subset of elements and compounds, but synthetic systems can be designed to use a wider range of elements and compounds, many of which would be toxic to most living organisms. Biological systems form and operate near room temperature in the presence of water and oxygen (for the most part), but synthetic systems can be formed and operate under a wide range of temperature and conditions. Finally, biological materials generally take days to years to form, but synthetic systems may be formed rapidly. For biology, systems that form slowly in response to external stimuli have significant advantages, for example, bone remodels to meet the demands of applied loads. However, in general, the long time scales required for formation of biological nanocomposites limit the application of direct biological synthesis of engineering materials to a few very specific cases.

Through self-assembly of organic molecules, biological systems have succeeded in synthesizing a wide range of composite and inorganic nanostructures. Biological systems contain large quantities of lipids, or soap-like molecules, which self-assemble (along with many other biological macromolecules, including proteins) to form the external membranes of cells, as well as smaller vesicles within the cell. These membranes serve to protect the interior contents, as well as to provide synthetic microreactors for biological processes. The concept of performing syntheses in self-assembled microreactors is in this sense biologically inspired, has been exploited by many researchers to create nanoparticles and composite nanostructures, and is the topic of this section.

The simplest examples of nanomaterials are zero-dimensional materials, known as 'nanoparticles'. The study of small semiconductor particles in general is of significant interest, because the electronic and optical properties of semiconductor nanoparticles change drastically as the characteristic dimension of a particle is reduced to the nanoscale regime, largely due to the quantum confinement of electrons within the particle, although surface-area effects may also play a role (Figures 3.11, 3.12) [50–52]. The most popular nanoparticles for basic studies have been II–VI semiconductor particles, because of their scientifically interesting and technologically important properties. In this context, synthetic methodologies for the formation of metal sulfide and selenide quantum dots and their assembly into higher-order structures have been widely studied [53–57]. For nanostructuring to dominate the properties of metal sulfides and other semiconductors, it is generally necessary for the characteristic dimension of the nanoparticle to be <10 nm [58]. Semiconducting nanoparticles are gener-

ally synthesized through one of three routes. The first, grinding of large chunks is rarely done for nanoparticle preparation, because the grinding process is poorly regulated, generally generating a very polydisperse population of particles, and grinding introduces too many contaminates for most applications. The other two methods, gas-phase and solution-phase synthesis, are much more common. Gas-phase synthesis is essentially a vaporization and condensation process – a crucible containing the desired semiconductor (or other material) is heated until it starts to sublime, and then an inert carrier gas is flowed over the material. The carrier gas then heads into a cool region where the gaseous semiconductor atoms or molecules condense into nanoparticles and are collected [59]. Although this method is fairly versatile, it operates only under conditions of high temperature and vacuum and generally produces solid spherical particles.

Solution-based synthetic routes for nanoparticle formation have ranged from simple precipitation reactions to much more complex self-assembly-based routes. In general, simple precipitation results in agglomerates of nanoparticles, and the size distribution generally varies widely. These problems led to research into synthetic procedures that would result in nanoparticles that are stable against aggregation and have narrow size distributions. A primary route to preventing both these problems is to use self-assembly-based techniques, which in many respects resemble nanostructure development in biological systems, including biomineralization, cell membrane development, and other biological structure formation. Solution-phase synthesis of semiconductors is often preferred over other techniques, because it is generally mild (even being carried out at room temperature and pressures) and can be used to create reasonable volumes of materials. Solution-phase synthesis has been widely used to grow semiconductor

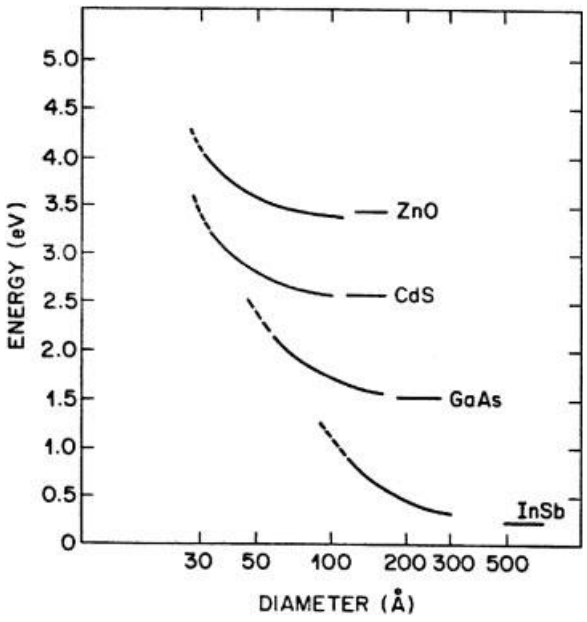

Fig. 3.11 Theoretical calculation of band-gap energy as a function of particle diameter for several different semiconductors. Adapted from [58]

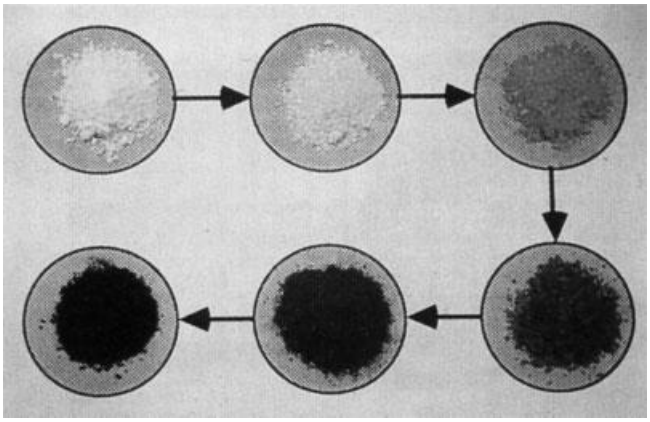

Fig. 3.12 Cd_3P_2 quantum dots. Particle size increases in the direction of the arrows. The white particles are about 1.5 nm, and the black particles are larger than 5 nm. Adapted from [50]

quantum dots, yielding particles with low polydispersities and novel optical properties [50, 51, 56, 57, 60]. Solution-based chemical syntheses are very attractive because they allow for direct control over the actual concentrations of the chemical precursors. Depending on actual conditions, it is even possible to cap the surface of the particles with organic molecules, which allows for further solution-based processing [53, 55].

The more conventional route to creating nanostructured materials is of course through top-down lithographic methods. Some examples of top-down techniques for generating very small features are extreme UV ($\lambda << 200$ nm) lithography [61, 62], electron beam writing [63], focused ion-beam lithography [64], x-ray-lithography [65], scanning probe lithography [66], and microcontact printing [67]. In general, all these techniques can form structures on the scale of tens to hundreds of nanometers, although generally only on very flat substrates, and they can be quite slow and often very expensive. The self-assembly-based route to nanostructure formation has the significant advantage that it is not limited to feature generation on flat surfaces, and it can be massively parallel. Of course, the general problem with self-assembly is that it is not possible to highly regulate the exact spatial position of the nanostructure, and thus we are still many years away from creating highly functional self-assembled electronic circuits.

In the micellar routes to nanoparticle formation, micelles are self-assembled from surfactant molecules and a solvent that contains at least one of the precursors for the inorganic nanoparticles in solution. The result is a solution that contains vast numbers of discrete nanoreactors which individually contain only a finite number of precursor species for the inorganic phase. When these ions are converted to mineral, generally by reduction or oxidation, the result can be one nanoparticle per micelle. The polydispersity in nanoparticle diameter is thus directly related to the polydispersity in the initial micelle size. If it were possible to create a suspension of monodisperse micelles, it would be a straightforward process to create nanoparticles with a very narrow size

distribution. Taking a lesson from biology, this might be possible through the use of complex macromolecules that organize into particles of only a specific size. A very good biological example of a potential nanoreactor with a tight size distribution is a virus particle. It may be possible to use virus particles to synthesize nanoparticles with tight size distributions if a way to load the interior of the virus particles with precursors for nanoparticles can be developed.

Most of the early nanoparticle synthesis routes produced solid semiconductor particles with morphologies never far from spherical. The creation of nanoparticles with complex morphologies is most interesting, because even such sophisticated patterning techniques as e-beam lithography are limited to ~10-nm features, which are often too large to result in the desired quantum confinement and other properties [63]. Nanoparticles having certain complex morphologies cannot be created through e-beam patterning or other top-down processing routes. The possibility of generating complicated

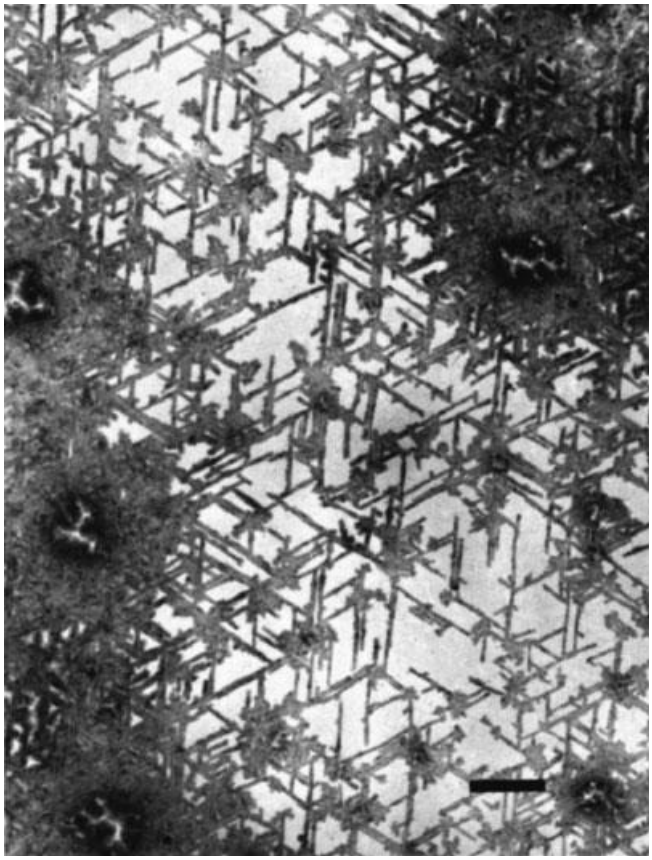

Fig. 3.13 Transmission electron micrograph of nanocrystalline CdS structure grown under an arachidic acid monolayer at room temperature. Scale bar = 200 nm. Adapted from [165]

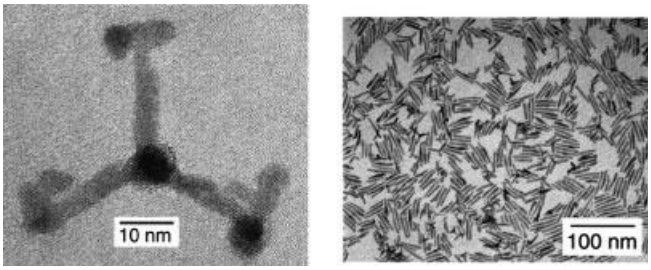

Fig. 3.14 Examples of CdSe nanoparticles with complex shape and form that can be created by solution synthesis from a mixture of surface passivating agents. Adapted from [70]

morphologies was examined in studies of CdS synthesized under Langmuir monolayers, in which dendritic structures were generated (Figure 3.13**)** [68]. Subsequently, a range of strategies have resulted in rod-like and even complex nanoparticles with complex morphologies that are based on self-assembly regulating the growth of semiconductor particles.

As examples of self-assembly processes which create nanoparticles with complex shapes, Alivisatos and coworkers [69, 70] demonstrated the formation of CdSe nanorods with aspect ratios of 30:1, as well as arrow-, teardrop-, tetrapod-, and branched tetrapod-shaped nanocrystals of CdSe (Figure 3.14). These highly shaped nanoparticles result from using a mixture of hexylphosphonic acid and trioctylphosphine oxide as passivating agents in the synthesis. Apparently, it is possible to block the growth of specific crystallographic faces while encouraging the growth of other faces. Thus, particles that have one crystallographic direction as their long axis, and their short axis as another crystallographic direction can be formed. The advantage of high aspect ratio particles over normal, spherical particles has not yet been proven, but the electronic or physical properties of the particles might be impacted by the change in shape. In addition, the particles might be able to self-assemble into higher-order structures because of their high aspect ratios; for example, they may form liquid crystalline phases, much like molecules with high aspect ratios [69, 70].

Semiconductor nanostructures may also have potential nonquantum confinement-based properties not found in the bulk equivalent. Besides quantum confinement, one way to greatly modify the properties of nanostructured semiconductors may be to design synthetic methodologies that result in dispersion of organic molecules within the inorganic phase at the molecular level. These composite materials could exhibit novel properties significantly enhanced over those of either the inorganic or organic phase alone, as has actually been observed in a wide range of materials. Composite materials that are tougher [71–73], have increased thermal stability [74], are electronically more sophisticated [75,76], or have enhanced chemical selectivity [77] than either of the constituent parts have been created. Even without the incorporation of organic material, periodically nanostructured semiconductors have great potential in solid-state science and technology, for example because of their potential for both electronic and catalytic activity. For example, a periodically nanostructured semicon-

ductor might behave as an array of antidots (a material with a regular array of scattering centers spaced closer than the mean free path of electrons traveling through them) [78, 79]. A nanostructural material is necessary because, if the mean free path of the electrons is shorter than the spacing between the scattering centers, the antidot lattice does not operate. At high magnetic fields (>2 Tesla), quantum steps in the conductivity as a function of electric field may be observed if the lattice spacing of the antidots is on the order of the cyclotron diameter of the electrons. In contrast to forming a solid of quantum dots, the formation of an antidot lattice requires the semiconducting structures to be continuous, with a periodic array of nanocavities.

Early on, the greatest emphasis was on creating nanoparticles with narrow size distributions, not on creating superlattice structures. However, through careful control of size distribution and chemical functionality, CdSe nanocrystals, and now many other nanocrystals, have been observed to order into superlattice structures [55]. These structures may present properties beyond simple quantum effects. The individual crystallites in this system do not form a continuous mineral structure, but are actually separated by thin layers of organic molecules, which are composed of the self-assembling molecules used in the synthesis to regulate the diameter and polydispersity of the particles. During synthesis, the organic self-assembles into a shell around the nanoparticles, imparting organic solubility to the nanoparticles, which enables them to be processed similar to organic compounds. Because of the high degree of regularity in size and shape, these organically coated nanoparticles assemble into a crystal of nanoparticles with long range periodicity, much in the way that organic molecules and atoms can crystallize.

The next level of complexity in nanostructure formation is the creation of nanostructures with complex, predefined morphologies. Here, the biological concepts of self-assembly and nanostructure formation become most applicable. For example, in biology, it is common to have complex predefined structures on the nanometer scale, yet this length scale is exceedingly difficult to regulate in synthetic materials. However, if the power of self-assembly is coupled with the materials synthesis strategies known today, there is great potential for the formation of complex composite nanostructures.

Liquid-crystal templating of inorganic nanostructures, an approach in which the periodic structure of liquid crystals is imparted to a mineral phase, is one such route. Liquid crystals present an ideal matrix for the creation of nanoscale composite materials, because the characteristic 1–10 nm length scales most often expressed in liquid crystals are similar to the size scale of interest for semiconductor nanostructures. Furthermore, the periodic structure in liquid crystals can be quite long-range, and thus the periodic nanostructure also has the potential for long-range order, which is of exceptional interest for many applications. A very important goal of several research groups is in fact the creation of long-range nanoperiodic order in materials such as semiconductors through liquid-crystal templating.

Semiconductors with long-range periodic composite structures could come in several forms, for example as a particle containing a periodic array of embedded second-phase material, as a thin film with a periodic topography, or as a periodically porous material. Highly porous, periodically nanostructured semiconductor particles could be

quite interesting for solution-based chemistry. For example, the photochemical nature of their semiconducting phase and zeolite-like pore structure could make them highly applicable for photochemical degradation of toxic compounds or for performing shape-selective chemistry, that is, chemistry that operates only on molecules of specific shape and size. Thin films may be even more technologically important, given the wide range of potential uses for both supported and freestanding thin films. The ability to predefine a nanoperiodic array of features in semiconductor thin films may open up many applications, including electronic devices, sensors, and filter membranes. Three-dimensional semiconductor structures may have unique optical or electronic properties, depending on the characteristic length scale of the structure. As the length approaches hundreds of nanometers, the materials may even exhibit photonic band-gap effects. Because direct top-down patterning of <10-nm-long nanostructures is difficult or impossible, and the patterning of 3D nanostructures of almost any length scale is difficult, templating of nanostructures through self-assembly processes has significant promise. Essentially, self-assembly-based templating can take place in either 2 or 3D, and the templating agent may or may not be removed, as desired. Here, we discuss several templating methodologies with potential for nanocomposite formation, the properties of such templated materials, and their potential applications.

3.4.1 Lyotropic Liquid-Crystal Templating

Lyotropic liquid-crystal templating is an approach for nanostructure and nanocomposite formation that utilizes the self-assembled structure of a liquid crystal to regulate the structure of a growing inorganic material. When processed correctly, the structure of the inorganic phase directly replicates the structure of the liquid crystal; thus the liquid crystal is a 'template' for the inorganic. The most important aspect of liquid-crystal templating of inorganic material is the lyotropic liquid crystal; thus, we should to review some of the basics of lyotropic liquid crystals. Lyotropic liquid crystals are composed of at least two covalently linked components, one of which is usually an amphiphile, which is a molecule that has two or more physically distinct components, and the other a solvent. Typically, one of the components making up the amphiphile is hydrophobic, and the other component is hydrophilic, as in common soaps, although this is not the necessary distinction. The dual solvent properties of an amphiphile lead to the interesting self-assembly of these molecules in solution by means that include surface segregation, formation of micelles [80,81] and vesicles [82,83], as well as the formation of a wide range of LC structures [84,85].

Most amphiphilic molecules contain two or occasionally three segments, of which at least one is water soluble. Clearly, if half a molecule dissolves in a solvent and the other half does not, interesting self-assembled structures may result. Within the general class of amphiphilic molecules are four distinct subclasses: cationic, anionic, zwitterionic, and nonionic. Cationic, anionic, and zwitterionic amphiphiles all contain a formally charged polar moiety, typically called the head group, and a nonpolar moiety, typically termed the tail. As the names imply, cationic amphiphiles contain a cationic

head group, such as a quaternary ammonium salt, and anionic amphiphiles, an anionic head group such as a sulfonate salt. Zwitterionic amphiphiles contain a head group having both positive and negative charge, for example trimethylammonium phosphonate. Nonionic amphiphiles do not contain charged functional groups, but instead contain polar segments such as oligo(ethylene oxide) or oligo(vinyl alcohol). Examples of anionic and nonionic amphiphiles, sodium octanoate and oligo(ethylene oxide) oleyl ether, respectively, are shown below.

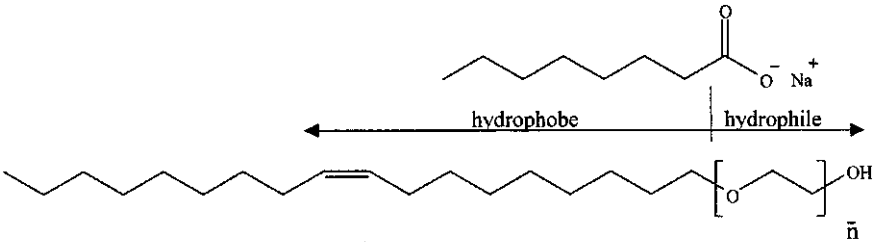

Amphiphiles exhibit very rich, complex phase behavior as a function of solvent concentration. In the dilute amphiphile limit, structures such as micelles form, and in the concentrated amphiphile limit (even solvent free), some amphiphiles show liquid crystalline or crystalline phases. Between these endpoints, a wide range of phases and structures can form. A typical nonionic amphiphile, oligoethylene oxide ($\overline{10}$) oleyl ether [(EO) $_{\overline{10}}$ oleyl], forms micelles, micellar rods, and hexagonal, cubic, and lamellar liquid crystals as the amphiphile:water ratio increases. This rich self assembling behavior occurs because the polar segment is readily solubilized by water, and the nonpolar tail is not. For a single molecule in solution, other than curling up on its self (which is entropically very unfavorable), there is no physical way to reduce the unfavorable interactions, but if multiple molecules are allowed to associate, or self-assemble, the unfavorable interactions can be reduced. Determination of the structure of this minimum-energy aggregate is beyond the scope of this book, but essentially one can calculate the free energies of each possible phase for a particular concentration and temperature and then select the lowest-energy phase [86].

The three most common phases observed in mixtures of water and amphiphile are hexagonal, lamellar and cubic. Correctly stated, the cubic phase encompasses a wide range of potential phases, all exhibiting cubic symmetry but with differing degrees of continuity in the hydrophilic or hydrophobic phases. Similar to the structures observed for block copolymers [87], the structures observed in lyotropic liquid crystals can be rationalized as a function of the volume fraction of the various components. Figure 3.15 shows representative phase diagrams for two nonionic amphiphiles: the first liquid crystalline phase observed as the amphiphile concentration is increased is the hexagonal phase, which is in essence the hexagonal close packing of rod-like micelles (Figure 3.16). These rod-like micelles develop in solution as the concentration of the amphiphile increases, but below a critical concentration do not pack closely. As the concentration of amphiphile is increased further, the spacing between the rod centers decreases, and eventually a critical point is reached where a bicontinuous cubic phase is formed (Figure 3.17). Finally, at high enough concentration of amphiphile, a lamel-

lar phase forms (Figure 3.18). In some systems, especially those composed of nonionic triblock amphiphiles, a close-packed cubic phase is observed, usually at lower concentrations of amphiphile than the hexagonal phase (Figure 3.19) [88, 89].

Rather then relying on coassembly, which is the process by which nanostructures develop in many mesoporous oxide systems, many biological processes utilize the order present in a preformed structure to form nanostructured inorganics. Substantial efforts have been made to utilize the order present in an organic mesophase to

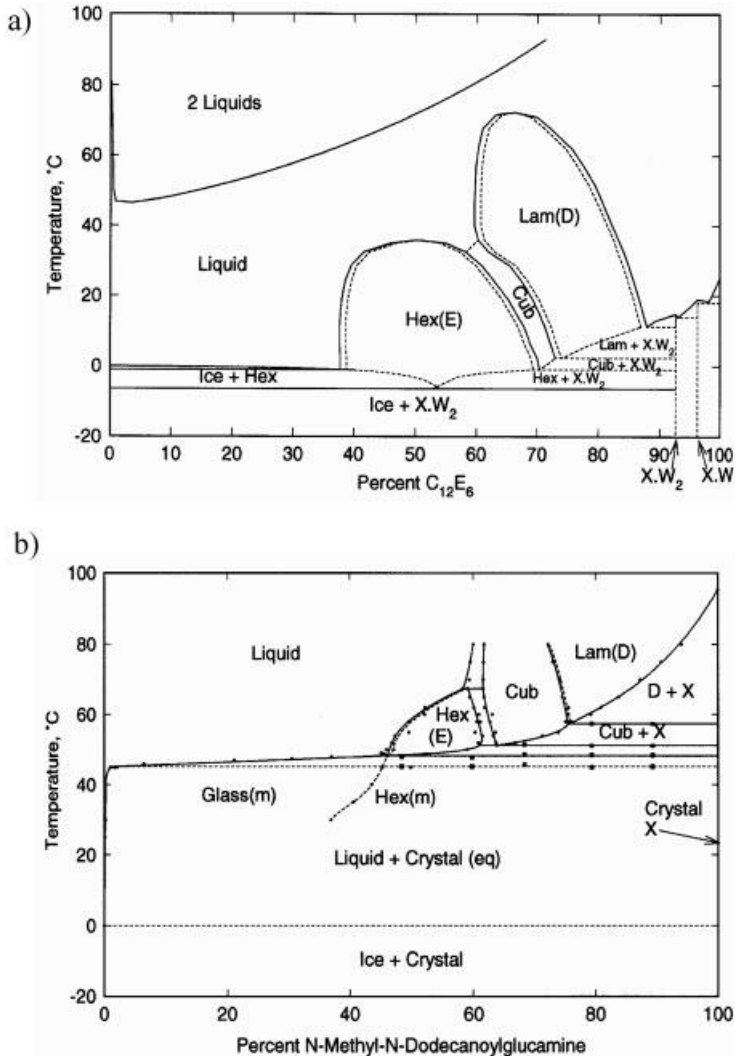

Fig. 3.15 Phase diagrams for nonionic amphiphile/water systems. (a) $C_{12}E_6$ (C_{12} represents the number of carbons in the tail, and E_6 represents the number of ethylene oxide groups in the head), (b) N-Methyl-N-dodecanoylglucamine. Adapted from [84]

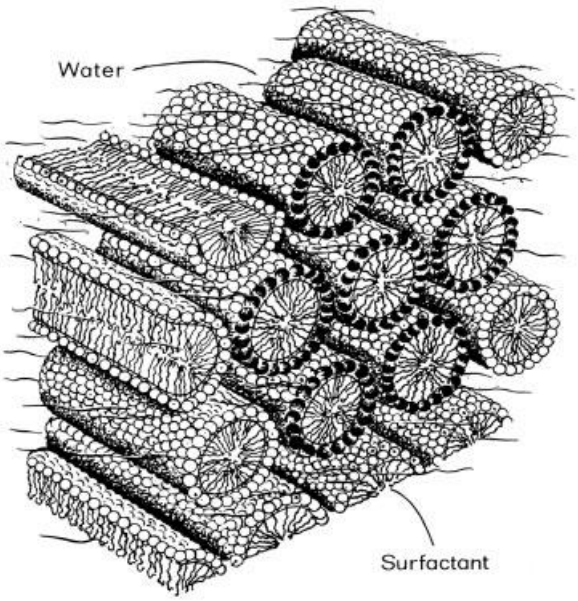

Fig. 3.16 Schematic illustration of the hexagonal phase. The polar head group of the surfactant points out into the water phase, and the hydrophobic tail inserts into the center of the rod-like micelles. Adapted from [166]

directly template the growth of an inorganic phase; liquid crystal templating has been one of the most successful of these approaches. Early efforts in this area resulted only in oblong or cubic crystallites or microporous reticulated structures [90–92]. More recently, through liquid-crystal templating, the successful synthesis of periodically nanostructured semiconductors that copied directly the symmetry and dimensionality of the precursor liquid crystal was demonstrated [11, 93–96]. Liquid-crystal templating appears to be a general route to the synthesis of semiconductor nanostructures. The general concept of liquid-crystal templating is to first form a liquid crystal that contains at least one of the precursors of the mineral phase, and then to induce a mineral phase to precipitate in only one chemical region of the liquid crystal by applying an outside

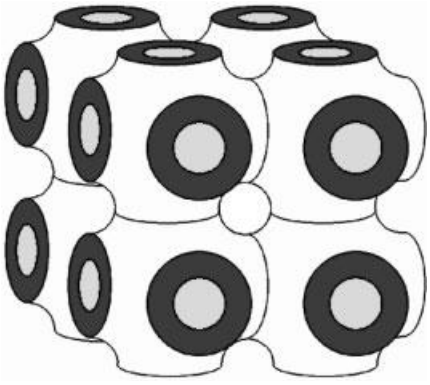

Fig. 3.17 Schematic illustration of a bicontinuous phase. The light gray region in the center of each circle indicates the hydrophobic segments, and the dark gray, the hydrophilic segments

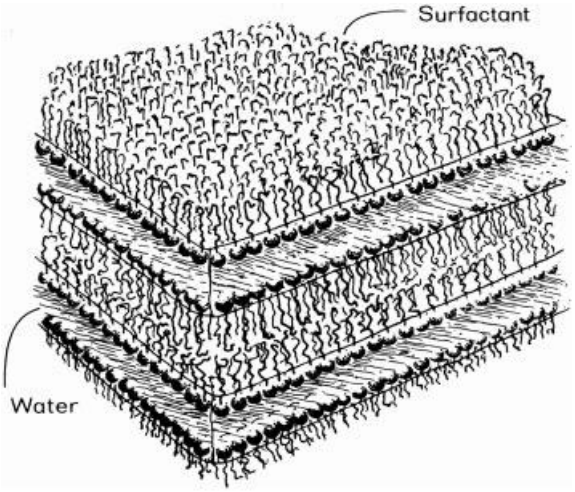

Fig. 3.18 Schematic illustration of the lamellar phase. Adapted from [166]

perturbation. Obviously, it is very important to select the correct synthetic conditions, mesophase, and mineral phase to be successful in this process. The versatility of this process has been demonstrated by the fact that materials have been formed in liquid-crystal phases, including the hexagonal, lamellar, and cubic phases, and the materials have included the already mentioned II–VI semiconductors; periodically nanostructured metals, both as thin films and in bulk [97–102]; as well as films of the chacogenides selenium and tellurium [103, 104]. Not only are the characteristic dimensions of the materials synthesized by liquid-crystal templating smaller than those obtainable

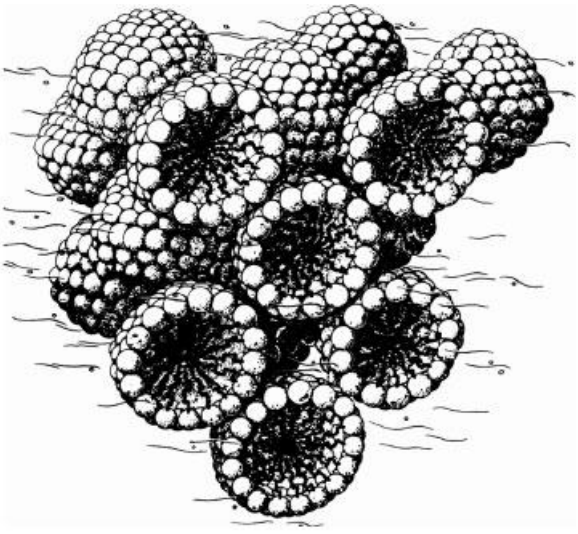

Fig. 3.19 Schematic illustration of the simple cubic phase. Adapted from [166].

by lithographic techniques, but they are often attainable through bulk synthesis, which is obviously not possible via lithography.

The direct templating of materials in the preordered environment of a nonionic amphiphilic mesophase generates semiconductor/organic superlattices containing both the symmetry and the long-range order of the precursor liquid crystal. In the templated growth of II–VI semiconductors, the semiconductor is grown in a water-containing liquid crystal by reaction of H_2S or H_2Se with a dissolved salt such as $Cd(NO_3)_2$. Both the chemical nature and the structure of the amphiphile are important for direct templating. For example, the order obtained in the nanostructured systems was even observed to be dependent on the counterion for the metal [95].

One advantage of direct templating with liquid crystals as a route to nanostructure formation, as was already discussed, is that there are a large number of amphiphilic liquid crystals, with lattice constants ranging from a few nanometers to tens of nanometers, and which include lamellar, hexagonal, cubic, and bicontinuous phases [84, 105, 106]. Potentially, many of these systems can be mineralized, generating materials with an array of novel structures and properties.

Specifically, II–VI semiconductors have been directly templated by hexagonal liquid crystals based on (EO) $_{\overline{10}}$ oleyl [11, 93, 95], and a lamellar liquid crystal formed from oligo(vinyl alcohol) ($\overline{23}$) oleyl ester [93]. As expected, the hexagonal liquid crystal

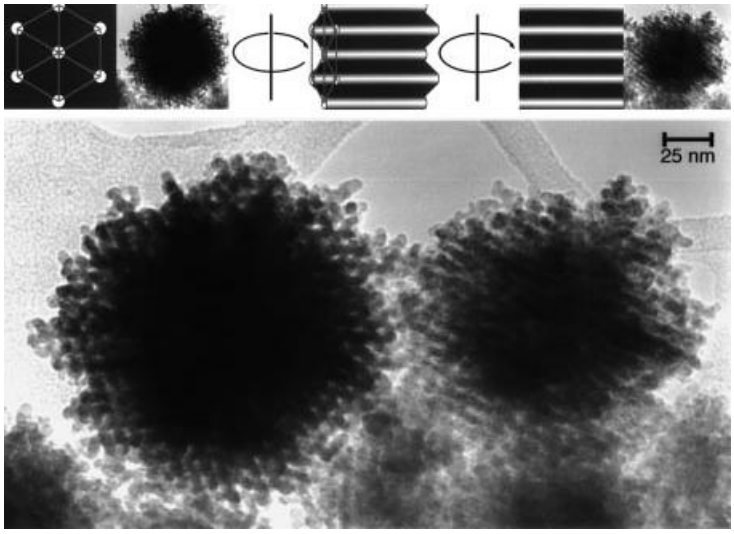

Fig. 3.20 The structure on the left in the transmission electron micrograph (bottom) is nanostructured CdS viewed with the hexagonally packed cylindrical templated pores parallel to the electron beam; the one on the right has the cylindrical structures perpendicular to the electron beam. Top: model of the nanostructure as a hexagonal arrangement of cylindrical pores of low electron density, corresponding to organic material in a solid matrix of semiconductor. The left and right schematic representations correspond to the adjacent micrographs; the central view shows the cylindrical assemblies in an intermediate state of rotation

yielded product with a hexagonal nanostructure, and the lamellar liquid crystal yielded a lamellar structure. (EO) $\overline{10}$ oleyl can also form a lamellar liquid crystal, which also was successful in templating a lamellar CdS product. Other lyotropic phases, such as a variety of bicontinuous and cubic liquid crystals [84, 105, 107], may also yield interesting mineral nanostructures. In this regard, CdS has been grown in a body-centered cubic phase by using a triblock copolymer of poly(oxyethylene)-poly(oxypropylene)-poly(oxyethylene) [(EO) $\overline{106}$ (PO) $\overline{70}$ (EO) $\overline{106}$] as the amphiphile. When mixed with water, the PO segment is only weakly solvated, but the EO is highly solvated. Thus, when this molecule is hydrated it forms micelles which pack closely, forming a cubic phase [106]. The result of precipitation in this cubic phase was the formation of hollow nanospheres of CdS, which are covered later in this chapter.

It is remarkable that a soft organic liquid crystal can directly template a hard covalent mineral phase. As a specific example, a hexagonal mesophase consisting of 50 vol. % aqueous 0.1 M $Cd(OAc)_2$ and 50 vol. % (EO) $\overline{10}$ oleyl templated an inorganic/organic nanocomposite of CdS and amphiphile when exposed to H_2S gas (Figure 3.20) [93]. The composite material contained an internal nanostructure that replicated the symmetry and dimensions of the liquid crystal in which it was grown. Interestingly, CdS and ZnS exhibited a superlattice morphology when formed in a liquid crystal from their respective nitrate salts and H_2S, but Ag_2S, CuS, HgS, and PbS did not (Figure 3.21). CdSe is also nanostructured by this method (Figure 3.22). An additional virtue of the (EO) $\overline{10}$ oleyl system is that, when combined with H_2O, it forms a hexagonal mesophase at 25 °C over the range of ~35 to ~65 vol. % amphiphile and a lamellar me-

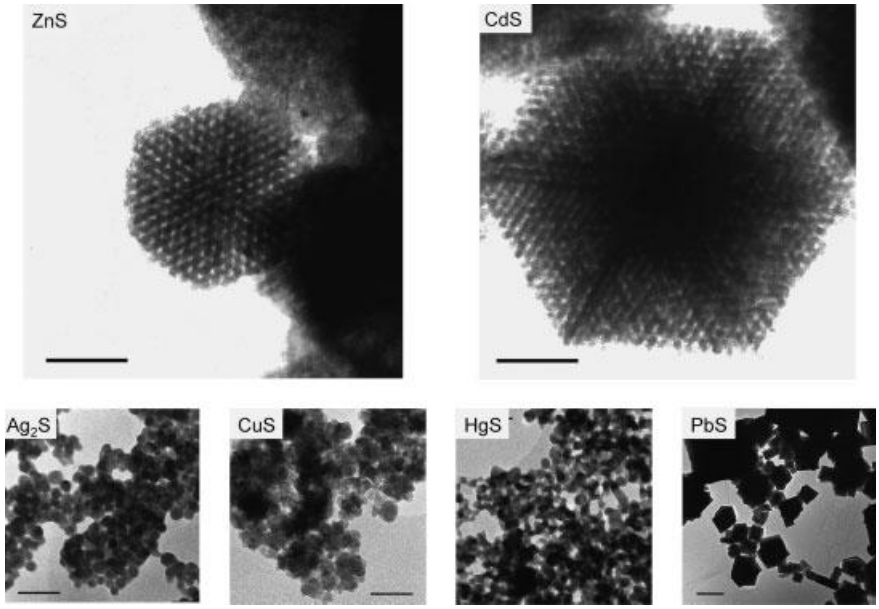

Fig. 3.21 Transmission electron micrographs of mineralized structures grown in hexagonal mesophases from their respective nitrate salt and H_2S (bar = 50 nm, except for PbS where the bar is 250 nm)

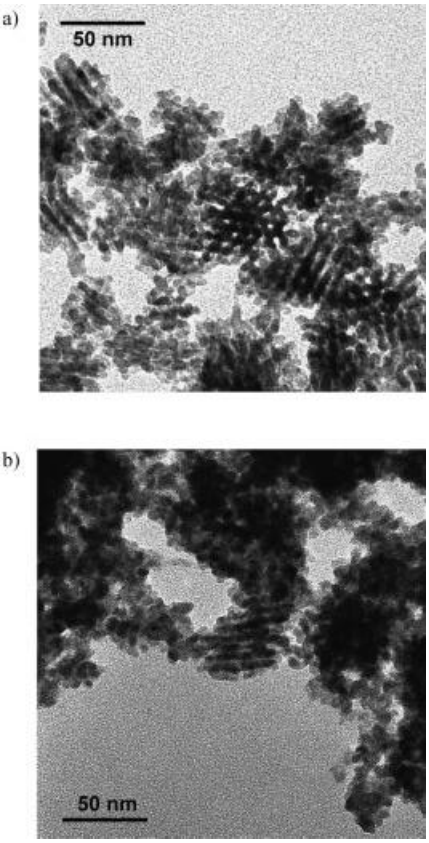

Fig. 3.22 Transmission electron micrographs of CdSe mineralized in hexagonal mesophases doped with (a) cadmium nitrate and (b) cadmium acetate

sophase from ~70 to ~85 vol. % amphiphile [108, 109], and it can directly template the growth of mineral over almost this entire range.

As shown in Figure 3.21, the nanostructures of the semiconductors CdS and ZnS synthesized by precipitation in hexagonal mesophases doped with their respective nitrate salts have hexagonal symmetry with a periodicity and dimensionality commensurate with that of the template. The hexagonal nanostructure is not always evident in TEM micrographs, due to random orientation of particles in the field of view. Presumably, if properly oriented, all the particles would show hexagonal symmetry. This was partially observed by tilting the samples on the TEM stage, revealing many more particles with hexagonal nanostructures.

CdS is also templated when grown from its acetate salt, although the order of its nanostructures is not nearly as well defined as in the nitrate systems (Figure 3.23) [95]. When ZnS is generated from its acetate salt, only spherical polycrystalline particles with a porous appearance are formed. Another difference between the product obtained from the acetate and nitrate salts is the average particle diameters of the semiconductor product: both CdS and ZnS grown from their respective nitrate salts are approximately five times larger than when grown from their acetate salts. This size

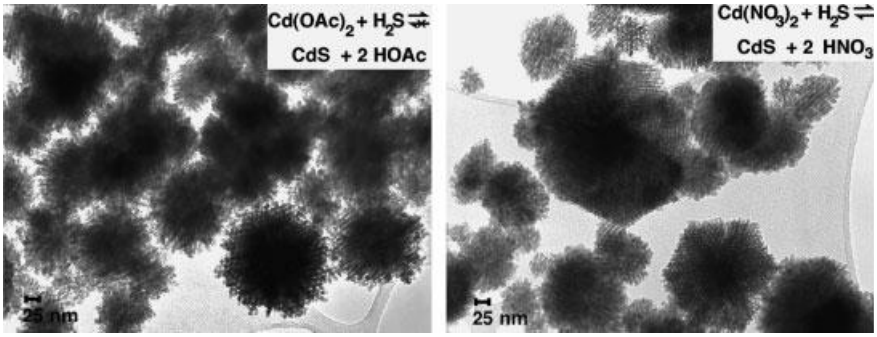

Fig. 3.23 Transmission electron micrographs of CdS grown in identical hexagonal mesophases except for precursor salt. Note the significantly improved order when cadmium nitrate is used as the precursor over the order obtained with cadmium acetate

difference can be clearly observed in low magnification electron micrographs. As controls, CdS was also grown in aqueous environments from both the nitrate and acetate precursors, and as expected, no nanostructure was generated. The counterion of the metal did not affect the templating of the other mineral systems studied: Ag_2S, CuS, HgS, and PbS were not generated with a superlattice morphology when grown in a hexagonal mesophase, irrespective of whether the acetate or nitrate salts were used. The reason may be that the byproduct of the synthesis from the nitrate salt is nitric acid, whereas the byproduct of the synthesis from the acetate salt is acetic acid. Nitric acid is a much stronger acid, and apparently enables the mineral phase to reform around the template during growth so as to remove any structural defects.

As already mentioned, in addition to the hexagonal mesophase, a lamellar mesophase of $(EO)_{\overline{10}}$ oleyl also can template a precipitated mineral (Figure 3.24). The la-

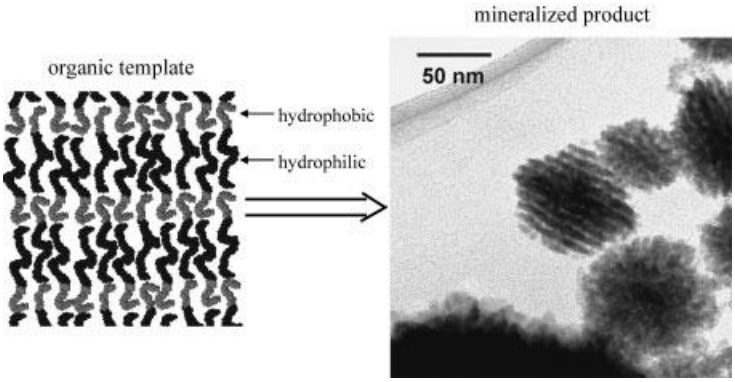

Fig. 3.24 Schematic representation of the lamellar organic template and transmission electron micrograph of the resulting product after mineralization. The dark bands are CdS that mineralized in the hydrophilic region of the template liquid crystal; mineral growth is prohibited in the hydrophobic regions

mellar periodicity in the resulting CdS is ~7 nm, which agrees very well with the periodicity of the lamellar template. The lamellar morphology can be confirmed by careful tilting of particles within the TEM. If a particle is tilted about an axis perpendicular to the stripes, no change is observed in the pattern. However, if it is tilted on an axis parallel to the stripes (and perpendicular to the electron beam), the pattern quickly disappears. These observations constitute strong evidence for a lamellar morphology within the particles and agree closely with results obtained from lamellar nanocomposites formed in a poly(vinyl alcohol)-based liquid crystal [94]. As shown in Figure 3.24, the mineralized product consists of disk-like particles with a long axis in the plane of the layers that is ~1.5 times the maximum width perpendicular to the layers. Very interestingly, particles having lamellar morphology do not disperse, even with repeated ultrasonication, perhaps due to mineral or organic bridging between the CdS layers. Presumably, CdS nucleates within a hydrophilic layer of the mesophase and grows rapidly in the plane, but concurrently an occasional finger forms perpendicular to this layer, piercing the hydrophobic region. This finger then nucleates another layer of CdS, resulting in a mineral bridge between layers. Another possibility is tethering of organic molecules in the mineral phase, tying the layers together. Of course, growth in the plane of the layers is faster than growth perpendicular to the layers, generating the disk-like habit observed. Not surprisingly, since it seems to enhance the templating effect, lamellar-nanostructured CdS was seen only when the nitrate salt was used, while the acetate salt afforded only small particles.

The layered structure formed by templating with a lamellar liquid crystal is in fact reminiscent of the layered abalone shell structure; however, in the templated material the characteristic dimension is just a few nanometers, not hundreds of nanometers to micrometers. It still remains to be seen if the properties of the layered material are significantly improved over those of the solid equivalent, but if the abalone shell is any guide, advanced mechanical properties are a possibility.

As described, mineral growth in the hexagonal and lamellar phases yields interesting, controlled nanostructures. Mineral growth in the cubic phase formed from (EO) $_{\overline{106}}$ (PO) $_{\overline{70}}$ (EO) $_{\overline{106}}$ was also done, using cadmium acetate and H_2S as precursors [110]. Although the mechanism is not entirely understood, the result was hollow spheres 20–200 nm in diameter (Figure 3.25), which can be observed by both TEM and SEM. When the sample is tilted in the stage, the shape and observed structure do not change, as expected for a hollow sphere (Figure 3.26). If the particles had been corpuscular in shape, their appearance would change as a function of sample tilt. The strongest evidence for their hollow nature is the dark edges of the spheres observed in TEM micrographs. If each sphere were solid, TEM would show greater scattering from the center than the edges, making the center appear darker. In the SEM, the spheres also scatter the most electrons from their edges and appear somewhat transparent in their centers, providing further proof of their hollow nature (Figure 3.25). Unlike materials produced by direct templating in hexagonal and lamellar liquid crystals, the hollow spheres are not of a size commensurate with the structure of the liquid crystal, but are rather 1–10 times the size of the characteristic dimension of the liquid crystal in which they were formed.

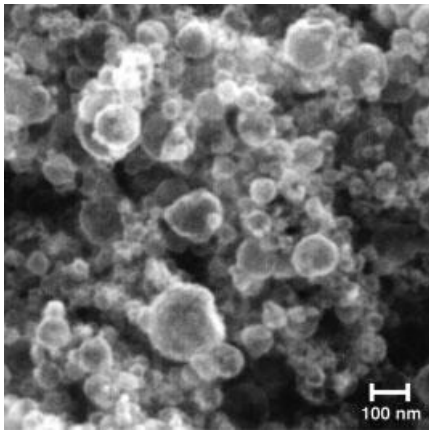

Fig. 3.25 Scanning electron micrograph of hollow spheres of CdS mineralized within a cubic mesophase

Because the characteristic dimension (diameter) for hollow CdS spheres obtained from the $Cd(CH_3CO_2)_2$-doped cubic phase is 20 – 200 nm, (1 – 10 times the diameter of the micelles making up the cubic phase), it does not appear that the mineral nanostructure is directly templated by the liquid crystal. In addition, this nanostructure is entirely absent from the CdS when the cubic phase is doped with $Cd(NO_3)_2$ as the precursor salt. This result is important when taken in the context of previous results in which the use of the nitrate salt led to a nanostructure with enhanced order [95]. In essence, the nitrate salt allowed the growing mineral to access a thermodynamically lower-energy morphology, which was a nanostructure commensurate with the structure of the liquid crystalline matrix. The inability of the nitrate salt to 'sharpen' the order in the cubic system is not surprising, because, as observed in previous studies, the nitrate salt only improves the registry between the nanostructure and the liquid crystal and does not result in a new nanostructure. In the cubic system, the spheres are not a copy of the liquid crystal, so there is no registry to improve. The mineralization of the cubic phase must lead to local rearrangements of the liquid crystal, leading to the hollow-sphere morphology observed; however, the detailed mechanism is still not understood.

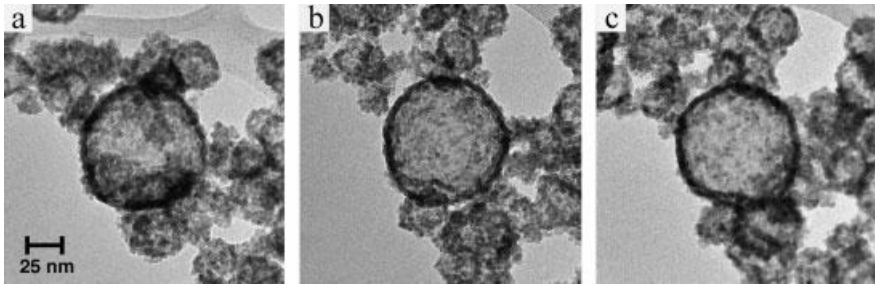

Fig. 3.26 Transmission electron microscope tilt series of hollow CdS spheres grown in an acetate-doped cubic phase. The tilt axis was diagonal running from upper left to lower right of each micrograph. (a) −45°, (b) 0°, (c) 45°

A potentially significant difference between the cubic phase and the other phases studied (hexagonal and lamellar) is the connectivity of the hydrophilic and hydrophobic portions of the liquid crystal. In the lamellar and hexagonal phases, both these regions are continuous in at least one direction. In the cubic phase, however, the hydrophobic regions are confined to discrete micelles. This confinement may cause a difference in templating ability relative to the other phases. For all templating phases, as the mineral nucleates and grows, it is necessary to expel some molecules from the volume occupied by the mineral. For both the lamellar and hexagonal phases, a molecule can diffuse away from the growing mineral without ever exposing its hydrophobic (oleyl) or hydrophilic (EO) segments to domains of the opposite nature. In contrast, in the cubic phase, when a molecule is forced away from the growing mineral it must leave its micelle and expose its hydrophobic (PO) segment to the polar surroundings (EO + H_2O), a high-energy situation. As already stated, the nitrate salt allows the mineral phase to access a lower-energy configuration, which in the lamellar and hexagonal systems results in a high degree of fidelity between the template and the semiconductor nanostructure. That a hollow-sphere morphology is not observed in the cubic system when the nitrate salt is used is not surprising, given that the hollow morphology is not directly templated by the liquid crystal and that formation of the spheres requires the mesophase to go through a high-energy intermediate state. The full reason for the spherical morphology when $Cd(CH_3CO_2)_2$ is used as the semiconductor precursor must be due to a subtle kinetic balance that is not yet understood. At the very least, the energy difference between the lamellar, hexagonal, and cubic systems is rather small, and thus the fact that templating is successful in the first two systems but unsuccessful in the last indicates that some fairly specific interactions are necessary for direct templating. This is similar to the action of many biological systems, in which very specific interactions between proteins and other macromolecules and growing inorganic phases are exceedingly important for structural development.

In addition to simple one-component systems, it is interesting to consider the result of templating binary mixtures of the precursor salts within a liquid crystal. In one system, a hexagonal mesophase containing 0.05 M $Cd(NO_3)_2$ and 0.05 M $Zn(NO_3)_2$ was mineralized. The resulting semiconductor ($Cd_xZn_{1-x}S$; $x \sim 0.5$) product's nanos-

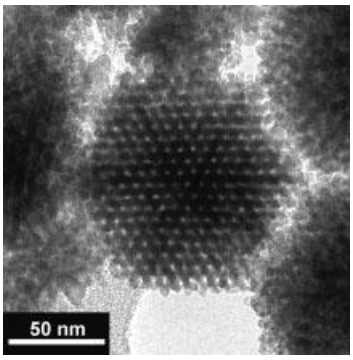

Fig. 3.27 Transmission electron micrograph of the product obtained from precipitation in a hexagonal mesophase doped with 0.05 M $Cd(NO_3)_2$ and 0.05 M $Zn(NO_3)_2$. The templated product is a solid solution of CdS and ZnS

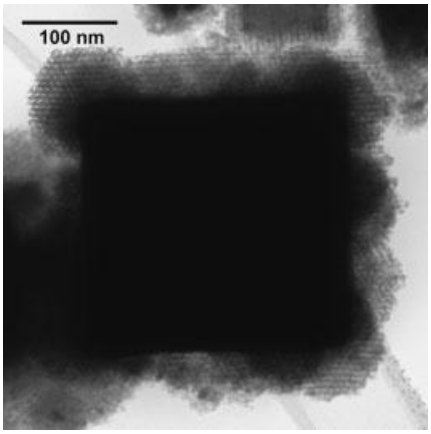

Fig. 3.28 Transmission electron micrograph of a composite product of PbS and ZnS grown in a hexagonal mesophase doped with 0.05 M $Pb(NO_3)_2$ and 0.05 M $Zn(NO_3)_2$. The single crystal cube at the core of the particle is PbS, and the shell is a periodically nanostructured solid consisting of ZnS

tructure exactly matched that of the template (Figure 3.27). In a system of 0.05 M $Pb(NO_3)_2$ and 0.05 M $Zn(NO_3)_2$, the result was a very different nanostructure, which consisted of a single-crystal core of PbS surrounded by a shell of nanostructured ZnS (Figure 3.28). From this it appears that, when mixed metal products are synthesized, there is a direct correspondence between the behavior of the constituent solids and the mixed solid. $Cd_xZn_{1-x}S$ was nanostructured (as were CdS and ZnS, Figure 3.21), but precipitation from Pb^{2+} and Zn^{2+} ions resulted in a single crystal of PbS surrounded by nanostructured polycrystalline ZnS, corresponding with the result seen for PbS and ZnS when grown discretely (Figure 3.21). The formation of mixed metal precipitates gives an insight into the growth processes and also opens the possibility of engineering a property. The system of $Cd_xZn_{1-x}S$ offers the possibility of band-gap engineering, although, due to the somewhat lower solubility of CdS than ZnS in water, the particles may be cadmium-rich in their center and zinc-rich on their exterior. The differing solubilities of PbS and ZnS in water play a very important role in the structure of the particles formed from this mixed system. PbS has a much lower solubility than ZnS and, as a result, upon exposure of the doped mesophase to H_2S, single-crystal PbS cubes nucleate and grow. Then, after most of the Pb^{2+} ions are locally exhausted, ZnS heterogeneously nucleates on the PbS particles. As expected, because ZnS is templated by liquid crystals, the shell of ZnS around the PbS single crystal contains a periodic superlattice structure.

Direct templating of an inorganic by an organic liquid crystal may depend on many factors, the most important of which is probably the thermodynamic stability of the mesophase throughout the mineral growth process. The mesophase must be stable to the addition of mineral precursors, and the mineral precipitation process must not disrupt the order of the liquid crystal. In studying direct templating, researchers have observed that the textures observed by polarized optical microscopy are the same for the pure mesophase and for a mesophase that contains the precursor salt, indicating that the doping did not lead to radical disruption of the order in the mesophase. Nuclear magnetic resonance (NMR) can also be utilized to verify the structure of liquid crystalline mesophases. To verify that the characteristic mole-

cular order of the mesophase was not disrupted by ion doping, broadline ^{2}H NMR spectra were obtained from both cadmium ion-doped and undoped mesophases [96]. For both mesophases, the same quadrupole splitting was observed (Figure 3.29). If ionic doping had perturbed the structure of the mesophase, the splitting would have decreased [111, 112]. As additional proof of molecular order in the mesophase, x-ray diffractograms were collected to characterize both the mesophase's long period and symmetry. For systems containing 35%, 40%, 50%, and 60% amphiphile, the 100, 110, and 200 reflections are clearly observed, indicating that the liquid crystalline structure is hexagonal (Figure 3.30). A mesophase containing 78% amphiphile forms a lamellar liquid crystal, as indicated by the presence of 100 and 200 reflections and the absence of a 110 reflection (Figure 3.31). As expected, a strong correlation was found between the phase diagrams as determined by optical analyses and the x-ray data. Similar experiments have been performed

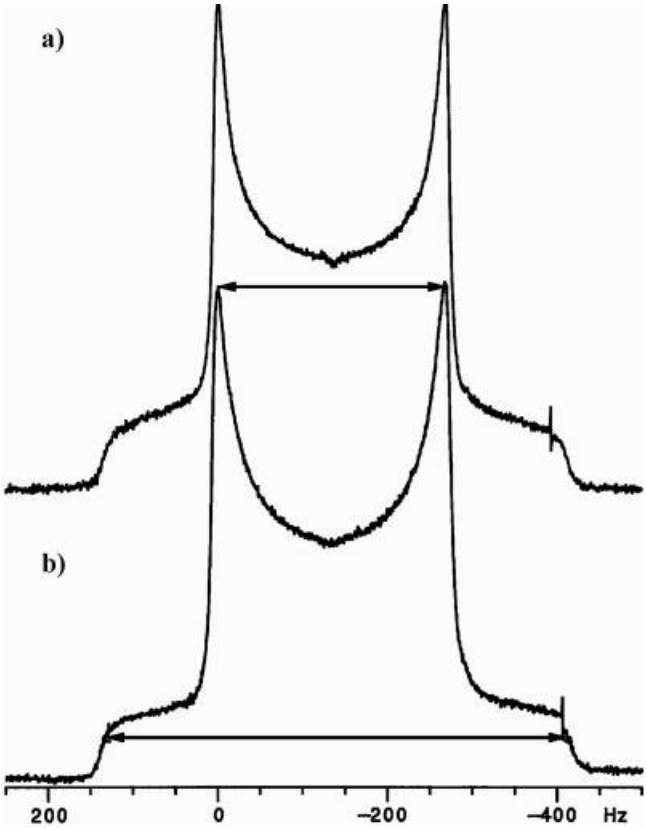

Fig. 3.29 Quadrupole splitting for a hexagonal mesophase (a) doped with 0.1 M cadmium acetate and (b) undoped. The splitting indicated by an arrow is the same for both samples

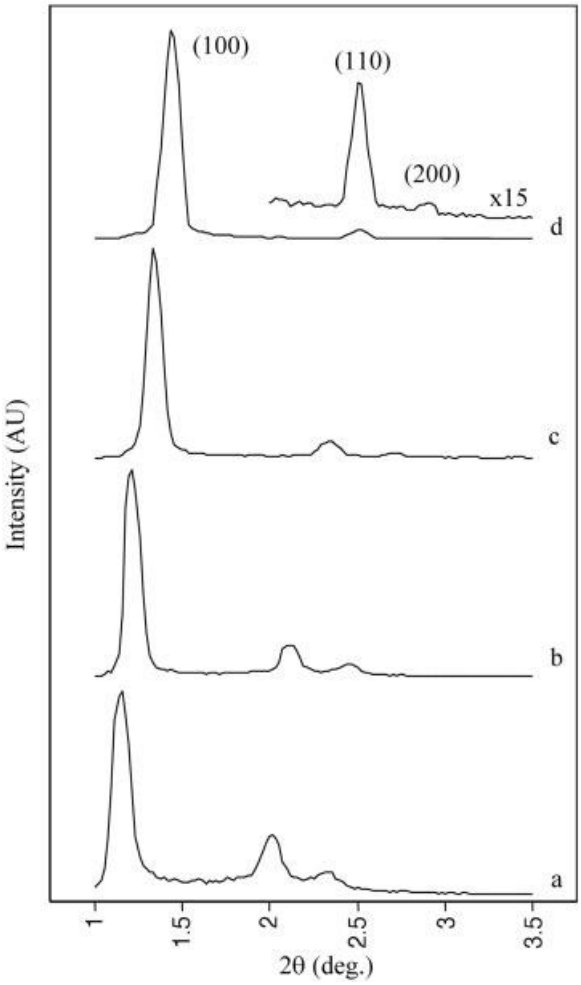

Fig. 3.30 Small-angle x-ray scattering of hexagonal aqueous mesophases containing (a) 35%, (b) 40%, (c) 50%, and (d) 60% amphiphile by volume

for other liquid-crystal templating systems, as well as for the formation of mesoporous silica.

In addition to the metal sulfides, which can be successfully templated as already mentioned, several sulfide materials, including Ag_2S, CuS, HgS, and PbS, were not templated by the liquid crystal in which they were grown, irrespective of the counterion. Design of amphiphiles with proper structures and binding constants for both the inorganic precursors and the inorganic product may enable a wide variety of inorganic and organic compounds to be templated in the future.

To better understand the scientific underpinnings of liquid-crystal templating, it is instructive to consider a few additional experiments. For example, liquid-crystal templating at elevated temperature sheds some light on the mesophase–ion–product interactions. As already mentioned, it appears the periodically nanostructured materi-

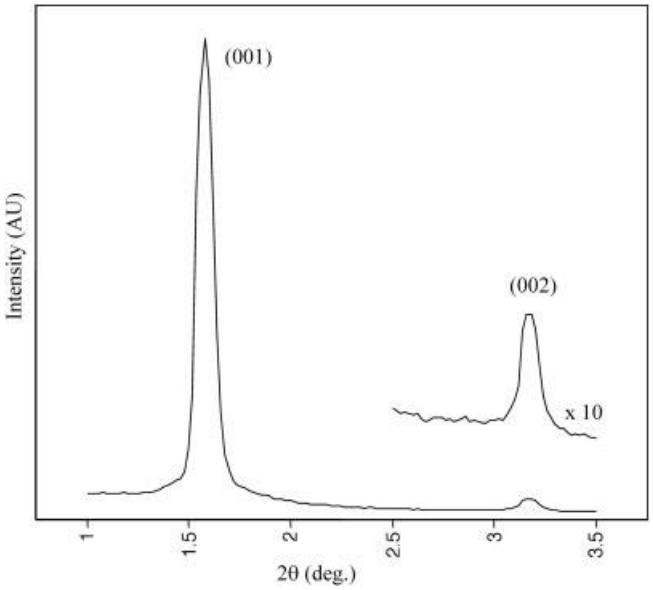

Fig. 3.31 Small-angle x-ray scattering of a lamellar mesophase containing 78% amphiphile and 22% water by volume

als are thermodynamically stable with respect to their solid equivalent. This implies that there is a critical energy balance between the energy gained by reducing the surface area of the mineral phase and the energy lost due to disruption of the mesophase structure. To study this further, CdS was precipitated in mesophases at both 35 °C and 50 °C. These temperatures are both below the isotropization temperature of the doped mesophases, so the reactions were carried out in a self-assembled medium. The CdS produced from the reaction at 35 °C did express the order of the mesophase, albeit poorly when compared with the order obtained at room temperature (22 °C). Precipitation at 50 °C resulted in mineral with no periodic order, clearly indicating that the energetic difference between periodically nanostructured and disordered product is small and that it only takes a small perturbation to result in nonnanostructured product.

As additional evidence for the direct templating mechanism, samples composed of 35%, 40%, 50%, and 60% by weight (EO) $\overline{10}$ oleyl were mineralized with CdS. By varying the amphiphile content of the mesophase, the spacing between the cylindrical aggregates of amphiphilic molecules making up the hexagonal mesophase was varied. Assuming that CdS is directly templated by the liquid crystal in which it is grown, the hexagonal symmetry and associated length scale should be nearly identical to that found in the precursor hexagonal mesophase, which is what indeed happened. The result (Figure 3.32), demonstrating that the superlattice dimension in the precipitate can be varied by changing the lattice constant of the mesophase, is very strong evidence for direct templating. If the nanostructure present in the templated inorganic phase had been the result of a cooperative self-assembly process, much as occurs for

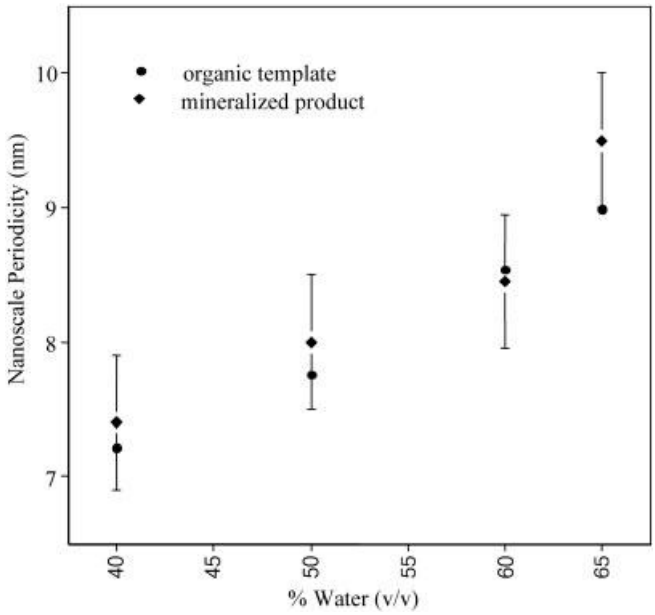

Fig. 3.32 Center-to-center spacing in a cylindrical assembly of amphiphilic molecules of hexagonal mesophases as determined by x-ray diffraction (●), and center-to-center pore spacing in templated CdS as measured by transmission electron microscopy (◆). Both are plotted as a function of the water content in the mesophase

most mesoporous silica systems, the result would have been that the periodicity of the nanostructure would not have changed with varying water content.

3.4.2 Liquid-Crystal Templating of Thin Films

The templating of thin films by self-organized organic structures should find significant application in both technology and scientific study. Thin-film templating is structurally related to the bulk templating of inorganic materials, which generally results in periodically structured particles; however, because the result is a periodically structured thin film, the potential for application is clearer. Templating with organic structures is especially intriguing because of the potential to create features much smaller than those feasible by almost any top-down technique, because it utilizes the nanoscale molecular order inherent in self-assembled organic structures to define the structure of the resulting thin film. A few key points must hold true for successful thin-film templating by liquid crystals. First, clearly, for templating to be successful, the self-assembled matrix must be compatible with the substrate. Then, via some process, the inorganic material must be deposited or grown on the substrate. Realistically, only chemical and electrochemical routes for materials deposition can meet these

requirements. Other conventional methods of thin-film deposition require high vacuum, which is incompatible with lyotropic liquid crystals and furthermore cannot operate through a thick overlying layer of liquid crystal.

The synthetic routes for liquid-crystal templating of thin films are relatively straightforward. To date, most studies have used electrochemical techniques to drive the material deposition. First, a precursor containing lyotropic liquid crystal is interfaced with the substrate. Then, under an applied potential, material is electrochemically deposited at the liquid-crystal/substrate interface. Nanostructured materials that have been created through this process include a variety of metals, selenium, and tellurium [97, 99–104, 113]. It may also be possible to electrodeposit other interesting materials including semiconductors; however, no publications have yet appeared demonstrating success.

Throughout, it is quite interesting that all the successful templating experiments have relied on liquid crystals formed of nonionic amphiphiles. However, in biology, most preformed matrices are formed via ionic macromolecules. In part, this is likely because biology makes use of very specific interactions to create mineral structures, but synthetic systems do not have this degree of sophistication. Thus, the fact that nonionic amphiphiles are much more stable to varying concentrations of soluble salts is actually an advantage. Ionic amphiphiles (as well as biomolecules) are affected much more strongly by salts, because a single salt ion can bind to one or more of the polar amphiphile headgroups, greatly reducing their polarity. This was indeed observed for several of the anionic amphiphiles studied, and most likely was the reason that ionic systems were not successful in templating the growth of a mineral phase. In biology, where the molecular structures are designed to interact specifically with one salt under very specific conditions, the strong interaction of ionic groups with dissolved species is an advantage. However, for generalized synthetic systems, this may not be an advantage.

3.4.3
Block-Copolymer Templating

Block copolymers are a widely studied class of materials that organize into both 2D and 3D structures at slightly longer length scales than observed for liquid crystals. Similar phase behavior is observed, with systems transitioning between lamellar, hexagonal and cubic phases as the relative volume fraction of the two blocks changes [87]. Much more complex morphologies can form in triblock systems. The characteristic periodicity in block copolymer systems ranges from ~5 nm to hundreds of nanometers and primarily depends on the molecular weight of the block copolymer. As expected, as the molecular weight of the block copolymer increases, the characteristic length scale increases. It was realized that if there was a way to impart this nanoscale order into a substrate, one might have a powerful technique for patterning materials with a periodic array of nanometer-sized structures. Unlike lyotropic liquid crystals, block copolymers are generally solvent-free and can be taken to elevated temperatures and under vacuum without destabilizing the self-assembled structure; thus high-vacuum mate-

rial deposition and processing approaches can be used. Usually the chemistry of the block copolymer is designed so that one of the two bocks can be removed via a dry etch with ozone or other reactive compound to generate the porous structure, which will subsequently serve as a template for nanostructure formation.

The procedure for block copolymer templating of nanostructures usually is as follows. A thin film of some block copolymer is spun-coated from solvent onto a substrate and allowed to self-assemble. After this, one of the blocks of the polymer is removed by ozone etching. The result of this etching procedure is a substrate coated with a thin polymer film containing a periodic nanoscale void structure. After removal of any solid polymer film that overlies the void structure, the polymer film is used as a mask. Material can be evaporated through the polymer film onto the substrate, material can be electrochemically grown from the substrate up through the polymer film, or the polymer film can be used as an etch mask. In all cases, the result is material structured to be a replica of either the polymer film (when the polymer is used as an etch mask) or the pore structure of the polymer film (when material is deposited in the pores). Usually, at the end, the polymer film is removed with solvent or reactive ion etch, leaving behind nanostructured templated features on a substrate. With this approach it is possible to create features as small as ~20 nm holes or dots in a periodic array on a substrate of a wide range of materials, including oxides, semiconductors, magnetic materials, and of course the polymer itself (Figure 3.33) [114–121]. The power of block copolymer templating is further enhanced due to the facts that both the size and spacing of the feature can be modulated simply by varying the molecular weight and composition of the polymer and that the lattice structure can be modulated by varying the relative length of the two blocks. For example, both the lamellar and hexagonal phases can template nanometer-scale lines if they are oriented

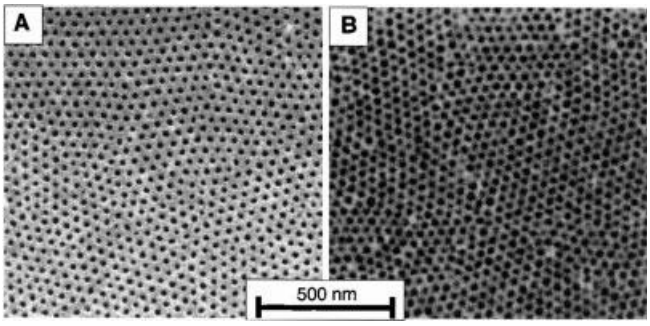

Fig. 3.33 (a) Scanning electron micrograph of a polystyrene/polyisoprene block copolymer template after it has been partially etched with ozone and the continuous polystyrene layer on the top has been removed. The now empty PI domains are now holes and are darker in the micrograph. (b) Scanning electron micrograph of hexagonally ordered arrays of holes in silicon nitride on a thick silicon wafer. This pattern is formed by using as a template a copolymer film such shown in (a). The darker regions are ~20-nm-deep holes in the silicon nitride layer, which are formed by etching through the overlying template. Adapted from [114]

properly on the substrate. I should point out that the periodic arrays of dots have attracted the greatest attention for applications such as magnetic storage media.

3.4.4 Colloidal Templating

In any discussion of biologically inspired nanocomposite materials, one must include recent developments on colloidal crystal templating of photonic materials. The basic premise behind this approach is to use the 3D periodic structure of synthetic opals to direct the structure of a second phase material. This approach is not biologically inspired, but should more accurately be described as 'naturally inspired', because opals, although natural, are geological, not biological, in origin. Furthermore, although the lower limit to the characteristic length scale of the material generated is 10–20 nm, the characteristic dimension is often relatively large, on the order of 500 nm. This is in fact intentional, since most of the applications for these materials are optical, and thus the characteristic length should not be much smaller than the wavelength of the light that one desires to modulate. Commonly, however, much smaller features are embedded within the templated structure, and these features may be as small as a few nanometers. Because of the clear natural inspiration for the colloidal templating of materials and the relationship of the templating process to many biological processes, I cover this approach in this chapter.

The interest in microperiodic 3D structures has grown tremendously due to the exciting potential of such materials, particularly in the area of photonics [122]. Such 3D structures, often termed photonic crystals, are the extension of the well-known dielectric stack into three dimensions. Although the colors that occur in opals, which stem from diffraction of white light by planes of highly ordered submicrometer silica spheres, are our inspiration; for practical application, synthetic approaches are needed to create materials and structures with the necessary refractive index and periodicity to meet the requirements for most optical applications, which opals simply do not have.

A particularly interesting class of optical structures are the so-called photonic band-gap materials. For example, a microperiodic material consisting of low-refractive-index spheres arranged in a face-centered-cubic array in a matrix with a high index of refraction, and having a lattice constant on the order of the wavelength of light (visible or infrared), could be such a photonic band-gap material [123]. Similar to how a dielectric stack has a stop-band for light in a given frequency range, this material would not allow light in a given frequency range to travel through it *in any direction*. In essence, it would be an omnidirectional, perfectly lossless, mirror.

The synthesis of these structures however is exceedingly difficult. Layer-by-layer fabrication of photonic crystals using state-of-the-art VLSI tools, e.g., deep UV photolithography, chemical vapor deposition (CVD), chemical-mechanical polishing, has been demonstrated [3], but formidable processing difficulties limit the formation of large area and truly 3D structures.

When appropriately formed, self-assembled colloidal crystals are natural candidates for the construction of photonic crystals. Good crystal quality is achieved only with

colloids that have very low size polydispersity (<5 %), which currently limits the choice of materials to SiO_2 or polymers, both of which have a fairly low index of refraction around 1.5, which is much smaller than that required for most optical applications. This has led researchers to take a two-stage templating approach. In a first step the desired microperiodic structure is assembled by using colloids. In a second step this structure is used as a template to build a complementary structure with a material having a higher index of refraction [124].

Colloidal crystal templating is a very promising approach for production of high-resolution, micrometer-scale, 3D periodic photonic crystals, but as conventionally applied to the fabrication of photonic band gap structures it has serious optical limitations, unless materials with the necessary optical properties can be used. Typically, the most important point is to infill with a material with a sufficiently high refractive index to generate an optically interesting material. A range of approaches have been suggested to maximize the index contrast, including sol–gel [125–127], chemical vapor deposition [128–131], imbibing of nanoparticles [132–134], reduction of GeO_2 to Ge [135], electroless [136] and electrochemical deposition [137], and melt imbibing [138]. In addition, polymers have been used to infill colloidal crystals, and in one report, the colloidal particles were less than 100 nm in diameter, which, although perhaps not interesting from an optical standpoint, may have potential for separation membranes and confined chemical reactor spaces [139]. Although they are not the focus of the following discussion, the colloidal templates used in these attempts are commonly polycrystalline and can contain unacceptably high numbers of defects; thus, substantial effort has also gone into creating colloidal crystals with low defect densities. Each of these infilling techniques has various advantages and disadvantages, which are discussed below. In general, they all consist of approaches to infill the interstitial space of the colloidal template, after which the colloidal template is generally removed.

The sol–gel infilling of colloidal crystal templates is intriguing to consider as a route to 3D porous materials [125–127], although it is somewhat limited in application for photonic materials for several reasons. First, the refractive index of most materials that can be formed via sol–gel is < 2 (with the exception of TiO_2, which can have a refractive index of $\sim$2.5), second, there is considerable reduction in volume during the conversion of the sol to solid material, and third, the refractive index of most sol–gel-derived material is substantially less than that of a single crystal of the same material. The net effect is that most sol–gel-derived macroporous materials have relatively low refractive index contrast, and their long-range order is somewhat disrupted due to the uneven contraction of the matrix. However, if one is not interested in photonic materials, but rather is attempting to make a ceramic macroporous material, sol–gel infilling of colloidal crystals may be a very good route. The contraction of the matrix may in fact be an advantage, in that it may be possible to make structures with pore diameters on the order of 50 % of the diameter of the template. Because it is difficult to make colloidal crystal templates from spheres smaller than a few hundred nanometers, this may be valuable for creating nanoperiodic structures.

Another pathway to macroporous materials is to fill the interstitial space of a colloidal crystal with nanoparticles, followed by removal of the colloidal template. This has some advantages over sol–gel infilling, in that the contraction of the structure

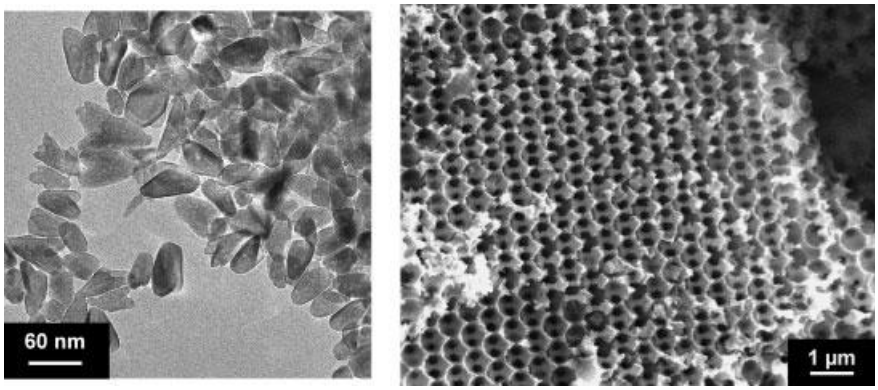

Fig. 3.34 Left, transmission electron micrographs of 3% erbium-doped hydrothermally synthesized titania nanoparticles. Right, scanning electron micrographs of macroporous titania structure formed by imbibing these nanoparticles into a colloidal template formed from 466 nm polystyrene colloidal particles. The colloidal template was removed by calcination at 300 °C for one hour in air

upon removal of the template from a nanoparticle filled colloidal crystal is significantly less than that seen upon removal of the template from a sol-gel filled system, and a much larger subset of materials can be prepared as nanoparticles, including semiconductors, metals, and ceramics. The first example of semiconductor nanoparticle infilling of colloidal template used II–VI semiconductor nanoparticles [132]; since then, Er-doped TiO_2 nanoparticles, for example, have been filled into a colloidal template, followed by removal of the template to generate a macroporous solid (Figure 3.34) [140].

The use of CVD as a pathway to filling colloidal crystals at first may seem counterintuitive. After all, CVD generally is most efficient at coating planar surfaces, and it would seem almost impossible to fill structures with deep pores, such as the interstitial space of a 3D colloidal crystal. However, significant strides have been made in the past few years, and now virtually complete infilling of colloidal structures with both Si and Ge via CVD has been demonstrated [128–131]. After dissolution of the colloidal template, the result is an inverse structure with the necessary refractive index and structural conditions to exhibit a complete photonic band gap.

Electrodeposition-based infilling is intriguing for several reasons and has the potential to be general with respect to both characteristic lattice constant and material (Figure 3.35). The potential for high-refractive-index materials, large area structures, and the complete infilling of thick 3D colloidal templates, as well as the low cost of electrodeposition have led to interest in this area. To date, three different classes of materials that have been electrodeposited into self-assembled colloidal crystals, namely semiconductors, polymers, and metals.

Semiconductors are interesting candidates for photonic crystals, primarily because of their high refractive indices and generally robust nature. For example, CdS has a refractive index of 2.5, and materials such as GaP, Si, and Ge have indices of 3.4, 3.5, and 4.0, respectively. However, routes to creating periodic macroporous structures

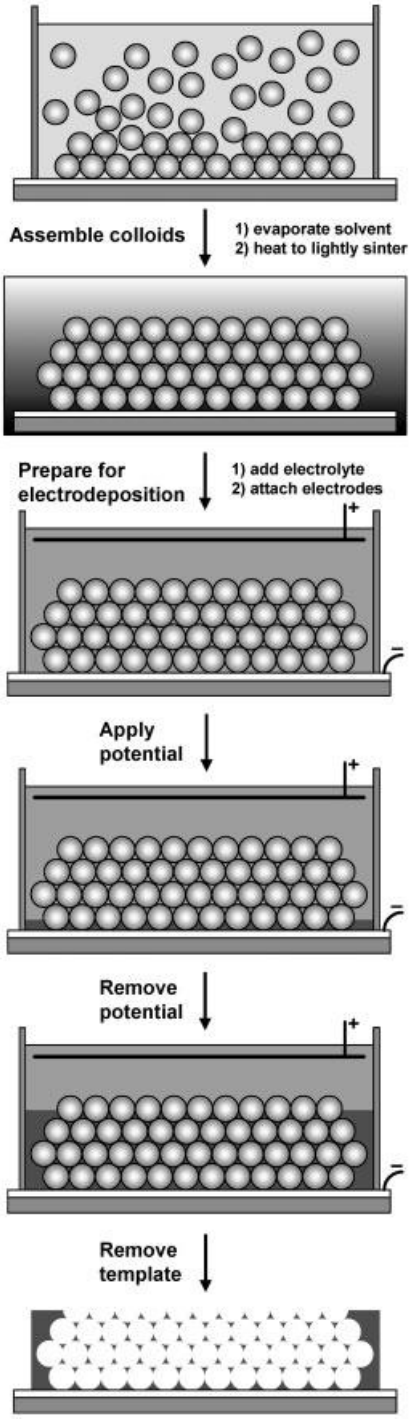

Fig. 3.35 Generalized procedure for creating 3D periodic macroporous materials by colloidal templating and electrodeposition. Monodisperse colloids sediment onto a conducting substrate, self-assembling into a crystal. The sample may be dried and sintered before electrolyte is added. A counterelectrode allows electrodeposition of the desired material (semiconductor, polymer, metal) into the interstitial spaces. In a final step the electrolyte and the templating colloid are removed. For polymeric colloids this can be done by treatment at elevated temperature or by dissolution with a solvent. For silica colloids, aqueous HF is effective for dissolving the template

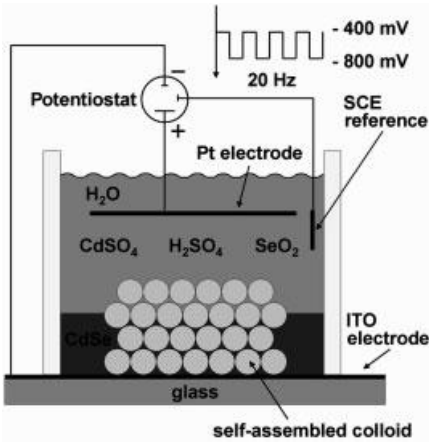

Fig. 3.36 Schematic representation of the experimental setup for potentiostatic deposition of CdSe through the interstitial space of a colloidal crystal

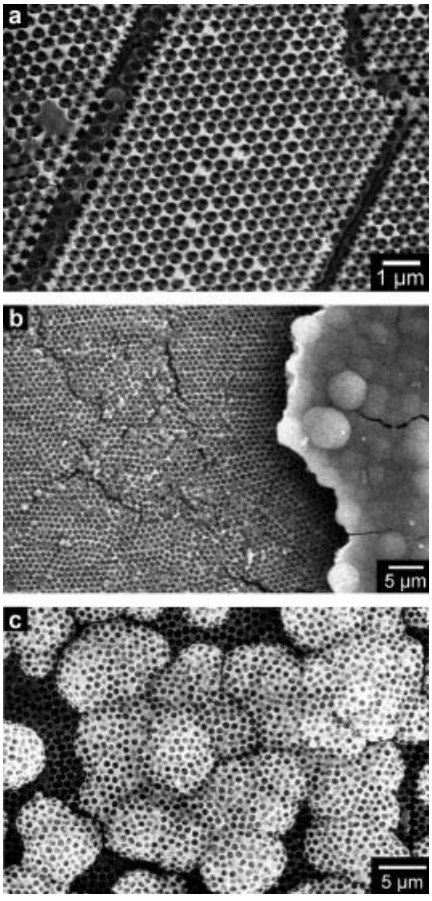

Fig. 3.37 Scanning electron micrographs of potentiostatically deposited CdSe (a) and galvanostatically deposited CdS (b, c) after removal of the polystyrene colloidal template. In the overdeposited system (b), the overlying solid CdS film can be clearly seen on the right. The apparent lack of periodic pore structure in the underdeposited system is not due to disorder in the colloid, but occurs because the nodular surface of the semiconductor cuts through multiple lattice planes of the template

from such materials are limited because of their very high melting points and low solubility in common solvents.

To date, the II–VI semiconductors CdS and CdSe [137, 141], and ZnO [142], have been electrochemically grown through colloidal templates, resulting, after dissolution of the template, in macroporous semiconductor films. For all systems, a conducting oxide film on glass was used as the substrate. Macroporous CdS films were generated by galvanostatic deposition through the interstitial spaces of a colloidal crystal formed from 1 μm SiO_2 spheres, and CdS and CdSe macroporous films were generated by potentiostatic deposition through a colloidal template generated from 466 nm polystyrene spheres (Figure 3.36). After electrodeposition, the SiO_2 and polystyrene colloidal templates were removed with aqueous HF and toluene, respectively. Because of the high rigidity of the semiconductor network, contraction upon removal of the template was limited to a few percent at most. The fine and gross morphologies of the electrodeposited semiconductors are shown in Figure 3.37.

Macroporous ZnO films were formed by potentiostatic deposition through a colloidal crystal formed from 368 nm polystyrene spheres, and the spheres were removed with toluene. Careful control of the electrodeposition conditions was necessary: if electrodeposition was done at a potential less negative than -1.0 V vs. Ag/AgCl, large crystalline grains of ZnO formed, which disrupted the structure of the colloidal template. Using a deposition potential more negative than -1.0 V suppressed the formation of large-grain ZnO, and the colloidal template was not disrupted.

All the electrodeposited semiconductor films are reported to be opalescent; however, detailed optical spectroscopy has yet to be performed. Real progress in optically interesting materials may await the electrochemical deposition of materials such as GaP, Ge, and Si, which, because they have refractive indices >3, may result in materials with 3D photonic band gaps. Routes to the electrodeposition of such materials have been demonstrated [143], but problems, such as hydrogen gas evolution and generally harsh conditions, need to be solved before success in these areas is likely.

Electrodeposition of conducting polymers (electropolymerization) through self-assembled colloidal crystals, followed by removal of the colloidal template, is a promising route to achieving active macroporous materials. Several significant advancements over the past few years have begun to demonstrate the potential of conducting polymer-based microperiodic photonic structures. Inherently, because of the low refractive index of polymeric materials, it is quite unlikely that a 3D photonic band-gap material will result from a polymer-based photonic crystal; however, conducting polymers have advantageous properties as compared to conventional polymers or inorganic materials: their optical properties can be electrochemically modulated, fine control over properties can be obtained through organic chemistry, and they are often mechanically flexible.

Electrochemical growth of conducting polymers is a fairly well developed field, and many procedures for growing solid films have been published [144]. There are, however, only a few reports on the growth of porous conducting polymer films. Fibers of polypyrrole, poly(3-methylthiophene), and polyaniline were formed in the early 1990s by electrodeposition from the appropriate monomer solution through a porous membrane [145]. The first example of electrochemical deposition of a conducting polymer

around a colloidal template was in 1992, when polypyrrole was grown around latex particles [146]. However, no attempt was made to remove the colloidal particles, and the optical properties of the resulting films were not measured. Only in the past few years have researchers been exploring the possibility of the templated growth of conducting polymers for photonic applications.

To date, three reports on colloidal templating of conducting polymers have appeared, all of which followed the general procedure of (1) colloidal crystal formation on a conducting substrate, (2) electrochemical deposition from solution, and (3) dissolution of the colloidal template with an appropriate solvent. In the first example, polypyrrole was grown potentiostatically from a solution of pyrrole in acetonitrile through a colloidal crystal composed of SiO_2 spheres with a mean diameter of 238 nm assembled on F-doped SnO_2-coated glass, followed by removal of the colloidal template with aqueous HF [147]. Macroporous polypyrrole, polyaniline, and polybithiophene films have been potentiostatically polymerized through a colloidal crystal assembled from 500 nm and 750 nm polystyrene spheres, on a substrate of gold-coated glass. The polystyrene template was then removed with toluene [148]. In the most recent example, polypyrrole and polythiophene macroporous films were potentiostatically grown through colloidal crystals assembled from 150 nm and 925 nm polystyrene spheres, respectively, on glass coated with indium tin oxide; the polystyrene was removed with tetrahydrofuran [149]. A preliminary optical characterization [149] showed a weak dip in transmittance that appeared to be correlated with the periodic structure.

One significant issue is the contraction of the period structure upon removal of solvent for electrodeposited macroporous polymers. This was most clearly observed in polystyrene-templated systems, in which significant contraction, ranging from 13% to 40%, was observed for the macroporous polypyrrole and polyaniline. However, very little contraction was observed in polystyrene-templated macroporous polybithiophene or when SiO_2 spheres were used as the template. For example, poly(ethylenedioxythiophene) was templated by silica colloidal particles (Figure 3.38). The primary difference is that organic solvents are used to remove the polystyrene spheres and an aqueous HF solution is used to remove the SiO_2 spheres. This suggests that the organic solvent softens the electrodeposited polymer, allowing it to contract; however, there may be other systems similar to polybithiophene, in which contraction of the macroporous matrix does not occur. This is less of a problem for macroporous metals and semiconductors.

Metallic macroporous ordered replicas of colloidal assemblies are of potential interest for a wide range of applications including filtration, separation, and catalysis. In addition, they might have interesting electrical, magnetic, or optical properties. The tools and techniques for electrochemically plating metals have been well established for thin films and even bulk materials. It is thus fairly straightforward to develop recipes to backfill the interstitial space of a colloidal self-assembled crystal with almost any metal.

From a photonic standpoint, the properties of bulk metals are very poor, although of course templated structures may have many other applications. The imaginary components of the dielectric constants of bulk metals are large, hence they readily absorb

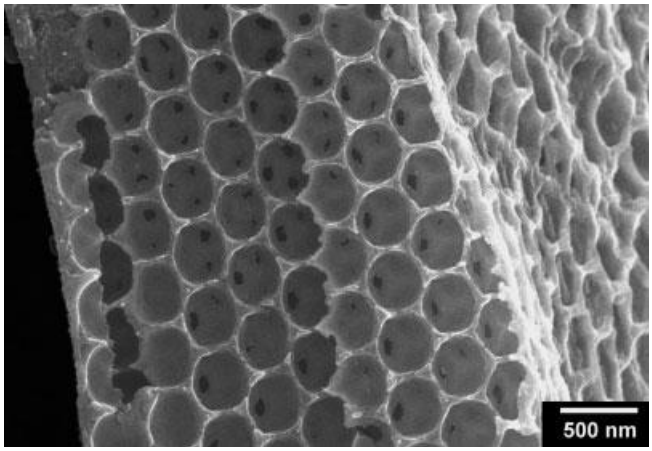

Fig. 3.38 Scanning electron micrograph of poly(ethylenedioxythiophene) electrodeposited around a colloidal crystal template, after dissolution of the template

light. When the metallic structures become small enough, however, strong optical resonances associated with plasmon frequencies of the conduction electron in the metals can lead to qualitatively new phenomena. A well-known example of this is the red color of a nanosized dispersion of gold colloid. A more recent manifestation of unexpected behavior is the anomalously high light transmission through small holes ($<$200 nm) in thin metallic films [150].

Theoretical calculations [151 – 153] on ordered 3D arrays of metallo-dielectric spheres show that these are promising for the construction of materials with full photonic band-gap in the visible part of the optical spectrum. The advantage of metallo-dielectric structures over purely dielectric structures is that it should be easier to achieve a full band-gap in the visible. A full band-gap in the visible is exceedingly difficult, if not impossible, to create with purely dielectric structures, because very few dielectric materials have an index of refraction >3 and very low absorption in the visible. This has led to the development of synthesis routes to produce metallo-dielectric colloidal core-shell particles with sizes in the submicrometer range [154, 155] and metallic shell thicknesses or cores that are small enough to show resonance effects.

Vos et al. [156] made gold replicas of colloidal crystals made of silica (radius 113 nm) and polystyrene (radius 322 nm). Prior to electrodeposition of the gold, the silica spheres were sintered by heat treatment at 600 °C. After electrodeposition of the gold, the silica template was removed by etching with aqueous HF, and the polystyrene spheres were removed by combustion at 450 °C (Figure 3.39). There are no dimensional changes between the dried, sintered colloid and the final replica, although some cracking is observed during the original drying and sintering process, indicating that the electrochemically formed gold is dense and structurally robust. This is a definite improvement over other methods of infilling macroporous structures with high-dielectric materials, e.g., liquid-phase or sol – gel chemistry [126, 127], and infiltration

with nanosized particles [132], in which considerable contraction of the matrix is observed, which leads to serious crack formation and warping of the colloidal structure. Other electrodeposited materials include Ni, Pt, and a SnCo alloy [157, 158], Pd, Pt, and Co [159]; electroless deposition has also been attempted [136].

As just described, recent work has demonstrated that templating of the interstitial space of highly ordered colloidal crystals has promise for creating macroporous photonic crystals from a diverse set of materials including oxides, semiconductors, metals, polymers, and glasses. The resulting 3D macroperiodic materials have been formed with close-packed macropores ranging in diameter from 100 nm to a few micrometers, giving the potential to modulate light ranging from deep UV to the infrared. However, problems with the infilling process still need to be overcome before this approach to photonic structures comes to fruition. As outlined, filling the 3D interstitial space of a colloidal crystal with a high-index material has been problematic, because many techniques either only deposit material in the top few layers of a colloidal crystal or do not fully fill the colloidal crystal with a material of high enough refractive index.

Another route to infilling of colloidal crystals to generate a high-refractive-index structure is melt-imbibing of a chalcogenide glass such as selenium, followed by dissolution of the silica template. Selenium was selected because it has a high refractive index of 2.5, and thus can provide a nearly complete 3D photonic gap (Figure 3.40), a very low optical loss coefficient between 1 and 10 μm [160], low melting point (217 °C), and relatively low surface tension ($\sim$100 dynes cm^{-1}), which reduces the force necessary to infill the structure. Importantly, selenium vitrifies easily, forming an optically isotropic glass [160]. Other chalcogenide glasses certainly could be used to infill colloidal crystals; however, they have higher softening points and thus are not suitable for initial investigation. Through melt imbibing, essentially complete infilling of a colloidal crystal was demonstrated (Figure 3.41).

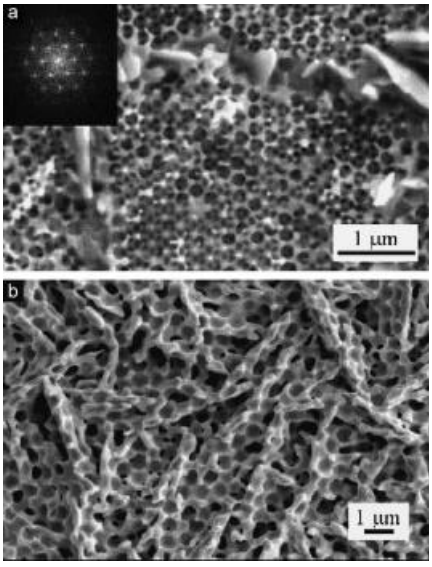

Fig. 3.39 (a) Scanning electron micrograph of a crystal of air spheres (radius 111 nm) in gold, made with a silica template. The inset is a Fourier transform of the image. (b) Scanning electron micrograph of macropores (radius 322 nm) in gold, made with a latex template. The structure has short-range order, but no long-range order. Adapted from [156]

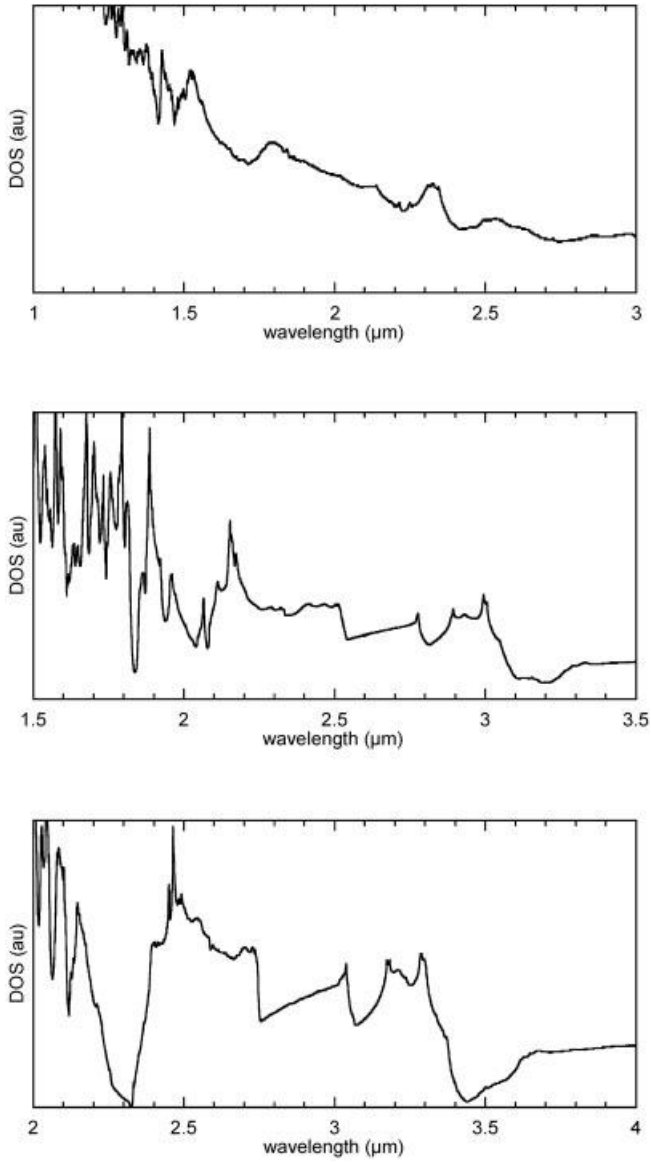

Fig. 3.40 Photonic density of states for inverse fcc structure for refractive index contrasts of (a) 1.45, (b) 2.5, and (c) 2.95; 1.45 corresponds to filling with a simple oxide such as silica, 2.5 to filling with selenium, and 2.95 to filling with a high-index chalcogenide glass such as $Ge_{25}As_{20}Se_{25}Te_{30}$. Note the deep photonic band gap for an index contrast of 2.5 at 2 μm and a complete gap at 2.3 μm for the system with an index contrast of 2.95. Adapted from [138].

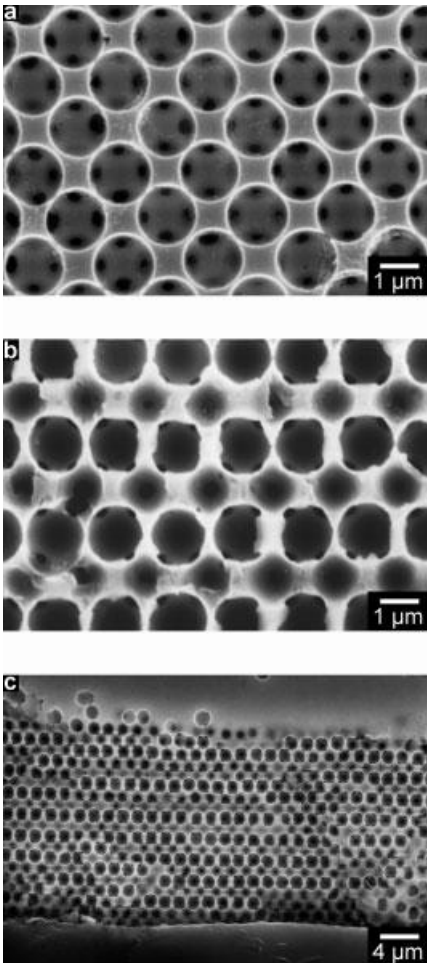

Fig. 3.41 Scanning electron micrographs of a selenium photonic crystal cut and polished to expose specific crystallographic faces. (a) Polished (001) facet, which is perpendicular to the settling direction. The contact points between the spheres on adjacent layers are clearly visible as pores, but within the (001) plane the voids do not appear to be interconnected. This pore morphology is the result of a 2% mismatch between the sphere diameter and the template size. (b) (110) face, proof that the selenium photonic crystal is indeed fcc. Again, the voids are generally not interconnected within the (001) plane, but are interconnected between (001) planes. (c) Low-magnification scanning electron micrograph of the (110) face, presenting a cross section of the entire thickness of the selenium photonic crystal. The sample was mounted in epoxy prior to polishing, which is seen below the photonic crystal; solid selenium is present above the photonic crystal. Importantly, the structure is highly ordered throughout the entire crystal, including the top layer. Because of an ~1.5° misorientation of the polished sample with respect to the (110) face, the size of the pores appears to change from left to right across the sample. Adapted from [138]

Infilling was accomplished by imbibing molten selenium under high pressure into the colloidal crystal, followed by quenching to vitrify the selenium. Subsequently, the colloidal crystal template was removed with HF, resulting in a macroporous selenium/air structure with a high contrast in refractive index.

3.5 Summary

The confluence of nanoscience, biotechnology, and materials chemistry offers great potential for discovery and fabrication of advanced composite materials. Great amounts of information still need to be gleaned from the study of biological systems, but we have now reached a point where the current body of knowledge on

how biological systems can create highly functional nanocomposites is starting to enable the creation of advanced materials. For example, natural systems widely exploit self-assembly to create a great diversity of interesting and highly functional materials, and today we are beginning to also create synthetic systems by similar processes. We must always remember that biological organisms work with a limited subset of materials and take up to years to create nanocomposite structures, so, rather than attempting to create materials by direct mimicking of biology, it will likely be much more productive to create materials by exploiting the design rules expressed by biological systems and applying them to synthetic systems. The dividends for research into biologically inspired nanocomposite materials are great, and much progress is expected in the near future.

References

1 Corma A: From microporous to mesoporous molecular sieve materials and their use in catalysis. Chem. Rev. 1997, 97:2373–2419.
2 Brinker CJ: Oriented inorganic films. Curr. Opin. Colloid Interface Sci. 1998, 3:166–173.
3 Soten I, Ozin GA: New directions in self-assembly: materials synthesis over 'all' length scales. Curr. Opin. Colloid Interface Sci. 1999, 4:325–337.
4 Antonietti M: Surfactants for novel templating applications. Curr. Opin. Colloid Interface Sci. 2001, 6:244–248.
5 Sayari A, Hamoudi S: Periodic mesoporous silica-based organic: inorganic nanocomposite materials. Chem. Mater. 2001, 13:3151–3168.
6 Stroscio JA, Eigler DM: Science 1991, 254:1319–1326.
7 Whitesides GM, Mathias JP, Seto CT: Molecular self-assembly and nanochemistry: a chemical strategy for the synthesis of nanostructures. Science 1991, 254:1312–1319.
8 Mann S, Ozin GA: Synthesis of inorganic materials with complex form. Nature 1996, 382:313–318.
9 Nanostructures: Special Issue: Nanostructured Materials. Chem. Mater. 1996, 8:1569–1882.
10 Stupp SI, LeBonheur V, Walker K, Li LS, Huggins KE, Keser M, Amstutz A: Supramolecular Materials: Self-organized nanostructures. Science 1997, 276:384–389.
11 Stupp SI, Braun PV: Molecular manipulation of microstructures: biomaterials, ceramics, and semiconductors. Science 1997, 277:1242–1248.
12 Liu J, Kim AY, Wang LQ, Palmer BJ, Chen YL, Bruinsma P, Bunker BC, Exarhos GJ, Graff GL, Rieke PC, et al.: Self-assembly in the synthesis of ceramic materials and composites. Adv. Colloid Interface Sci. 1996, 69:131.
13 Shenton W, Pum D, Sleytr UB, Mann S: Synthesis of cadmium sulfide superlattices using self-assembled bacterial S-layers. Nature 1997, 389:585–587.
14 Neeraj, Rao CNR: Metal chalcogenide-organic nanostructured composites from self-assembled organic amine templates. J. Mater. Chem. 1998, 8:279–280.
15 Schnur JM: Lipid Tubules: A paradigm for molecularly engineered structures. Science 1993, 262:1669–1676.
16 Archibald DD, Mann S: Template mineralization of self-assembled anisotropic lipid microstructures. Nature 1993, 364:430.
17 Kresge CT, Leonowicz ME, Roth WJ, Vartuli JC, Beck JS: Ordered mesoporpous molecular sieves synthesized by a liquid-crystal template mechanism. Nature 1992, 359:710–712.
18 Beck JS, Vartuli JC, Kennedy GJ, Kresge CT, Roth WJ, Schramm SE: Chem. Mater. 1994, 6:1816–1821.
19 Monnier A, Schuth F, Huo Q, Kumar D, Margolese D, Maxwell RS, Stucky GD, Krishnamurty M, Petroff P, Firouzi A, et al.: Cooperative formation of inorganic-or-

ganic interfaces in the synthesis of silicate mesostructures. Science 1993, 261:1299–1303.
20 Huo Q, Margolese DI, Ciesla U, Feng P, Gier TE, Sieger P, Leon R, Petroff PM, Schuth F, Stucky GD: Generalized synthesis of periodic surfactant/inorganic composite materials. Nature 1994, 368:317–321.
21 Firouzi A, Kumar D, Bull LM, Besier T, Sieger P, Huo Q, Walker SA, Zasadzinski JA, Glinka C, Nicol J, et al.: Cooperative organization of inorganic-surfactant and biomimetic assemblies. Science 1995, 267:1138–1143.
22 Attard GS, Glyde JC, Goltner CR: Nature 1995, 378:366–368.
23 Beck JS, Vartuli JC: Curr. Opin. Solid State Mater. Sci. 1996, 1:76.
24 Hinman MB, Jones JA, Lewis RV: Trends Biotechnol. 2000, 18:374.
25 Hayashi CY, Shipley NH, Lewis RV: Int. J. Biol. Macromol. 1999, 24:271.
26 Gosline JM, Guerette PA, Ortlepp CS, Savage KN: J. Exp. Biol. 1999, 202:3294.
27 Hayashi CY, Lewis RV: Science 2000, 387.
28 Thiel BL, Viney C, Jelinski LW: β sheets and spider silk. Science 1996, 273:1477–1480.
29 Simmons AH, Michal CA, Jelinski LW: Molecular orientation and two-component nature of the crystalline fraction of spider dragline silk. Science 1996, 271:84–87.
30 Lazaris A, Arcidiacono S, Huang Y, Zhou J-F, Duguay F, Chretien N, Welsh EA, Soares JW, Karatzas CN: Spider silk fibers spun from soluble recombinant silk produced in mammalian cells. Science 2002, 295:472–476.
31 Harrison CC: Evidence for intramineral macromolecules containing protein from plant silicas. Phytochem. 1996, 41:37–41.
32 Mann S: Biomineralization: Principles and Concepts in Bioinorganic Materials Chemistry. Oxford: Oxford University Press; 2002.
33 Schultze-Lam S, Harauz G, Beveridge TJ: Participation of a cyanobacterial S layer in fine-grain mineral formation. J. Bacteriol. 1992, 174:7971–7981.
34 Schultze-Lam S, Fortin D, Davis BS, Beveridge TJ: Mineralization of bacterial surfaces. Chem. Geol. 1996, 132:171–181.
35 Weiner S, Addadi L: Design strategies in mineralized biological materials. J. Mater. Chem. 1997, 7:689–702.
36 Weiner S, Traub W, Wagner HD: Lamellar bone: structure–function relations. J. Struct. Biol. 1999, 126:241–255.
37 Weiner S, Wagner HD: The material bone: structure mechanical function relations. Annu. Rev. Mater. Sci. 1998, 28:271–298.
38 Douglas K, Clark NA, Rothschild KJ: Nanometer molecular lithography. Appl. Phys. Lett. 1986, 48:676–678.
39 Douglas K, Clark NA, Rothschild KJ: Biomolecular/solid-state nanoheterostructures. Appl. Phys. Lett. 1990, 56:692–694.
40 Coffer JL, Bigham SR, Li X, Pinizzotto RF, Rho YG, Pirtle RM, Pirtle IL: Dictation of the shape of mesoscale semiconductor nanoparticle assemblies by plasmid DNA. Appl. Phys. Lett. 1996, 69:3851–3853.
41 Mirkin CA, Letsinger RL, Mucic RC, Storhoff JJ: A DNA-based method for rationally assembling nanoparticles into macroscopic materials. Nature 1996, 382:607–609.
42 Alivisatos AP, Johnsson KP, Peng XG, Wilson TE, Loweth CJ, Jr, Bruchez MP, Schultz PG: Organization of 'nanocrystal molecules' using DNA. Nature 1996, 382:609–611.
43 Alivisatos AP, Schultz PG, Peng XG, Loweth CJ, Caldwell WB: DNA-based assembly of gold nanocrystals. Angew. Chem., Int. Ed. Engl. 1999, 38:1808–1812.
44 Soto CM, Srinivasan A, Ratna BR: Controlled assembly of mesoscale structures using DNA as molecular bridges. J. Am. Chem. Soc. 2002, 124:8508–8509.
45 Brown S: Engineered iron oxide-adhesion mutants of the Escherichia coli phage-lambda receptor. Proc. Natl. Acad. Sci. U.S.A. 1992, 89:8651–8655.
46 Brown S: Metal recognition by repeating polypeptides. Nat. Biotechnol. 1997, 15:269–272.
47 Whaley SR, English DS, Hu EL, Barbara PF, Belcher AM: Selection of peptides with semiconductor binding specificity for directed nanocrystal assembly. Nature 2000, 405:665–668.
48 Lee SW, Mao CB, Flynn CE, Belcher AM: Ordering of quantum dots using geneti-

cally engineered viruses. Science 2002, 296:892–895.
49 Addadi L, Weiner S: Control and design principles in biological mineralization. Angew. Chem., Int. Ed. Engl. 1992, 31:153–169.
50 Weller H: Colloidal semiconductor Q-particles: chemistry in the transition region between solid state and molecules. Angew. Chem., Int. Ed. Engl. 1993, 32:41–53.
51 Weller H: Quantized semiconductor particles: a novel state of matter for materials science. Adv. Mater. 1993, 5:88–95.
52 Weller H: Optical properties of quantized semiconductor particles. Philos. Trans. R. Soc. London, Ser. A 1996, 354:757–766.
53 Murray CB, Norris DJ, Bawendi MG: J. Am. Chem. Soc. 1993, 115:8706.
54 Dabbousi BO, Murray CB, Rubner MF, Bawendi MG: Langmuir–Blodgett manipulation of size-selected cdse nanocrystallites. Chem. Mater. 1994, 6:216–219.
55 Murray CB, Kagan CR, Bawendi MG: Self-organization of CdSe nanocrystallites into three-dimensional quantum dot superlattices. Science 1995, 270:1335–1338.
56 Alivisatos AP: Semiconductor nanocrystals. MRS Bull. 1995, 20:23–32.
57 Peng X, Wilson TE, Alivisatos AP, Schultz PG: Synthesis and isolation of a homodimer of cadmium selenide nanocrystals. Angew. Chem., Int. Ed. Engl. 1997, 36:145–147.
58 Brus LE: Electron–electron and electron–hole interactions in small semiconductor crystallites: the size dependence of the lowest excited electronic state. J. Chem. Phys. 1994, 80:4403–4409.
59 Siegel RW: Creating nanophase materials. Sci. Am. 1996, 275(December):74–79.
60 Fendler JH, Meldrum FC: The colloid chemical approach to nanostructured materials. Adv. Mater. 1995, 7:607–632.
61 Geppert L: Semiconductor lithography for the next millennium, IEEE Spectrum 1996, 33: 33–38.
62 Levenson MD: Solid State Technol. 1995 (Sept) 81.
63 Chang THP, Thomson MGR, Yu ML, Kratschmer E, Kim HS, Lee KY, Rishton SA, Zolgharnain S: Microelectron. Eng. 1996, 32:113.
64 Matsui S, Ochiai Y: Nanotechnology 1996, 7:247.
65 Smith HI, Schattenburg ML, Hector SD, Ferrera J, Moon EE, Yang IY, Bukhardt M: Microelectron. Eng. 1996, 32:143.
66 Marrian CRK, Snow ES: Microelectron. Eng. 1996, 32:173.
67 Zhao X-M, Xia Y, Whitesides GM: J. Mater. Chem 1997, 7:1069.
68 Fendler JH: Membrane-Mimetic Approach to Advanced Materials. Berlin: Springer-Verlag; 1994.
69 Peng XG, Manna L, Yang WD, Wickham J, Scher E, Kadavanich A, Alivisatos AP: Shape control of CdSe nanocrystals. Nature 2000, 404:59–61.
70 Manna L, Scher EC, Alivisatos AP: Synthesis of soluble and processable rod-, arrow-, teardrop-, and tetrapod-shaped CdSe nanocrystals. J. Am. Chem. Soc. 2000, 122:12700–12706.
71 Berman A, Addadi L, Weiner S: Nature 1988, 331:546–548.
72 Berman A, Addadi L, Kvick A, Leiserowitz L, Nelson M, Weiner S: Science 1990, 250:664–667.
73 Berman A, Hanson J, Leiserowitz L, Koetzle TF, Weiner S, Addadi L: Science 1993, 259:776–779.
74 Messersmith PB, Stupp SI: High-temperature chemical and microstructural transformations of a nanocomposite organoceramic. Chem. Mater. 1995, 7:454–460.
75 Mitzi DB, Feild CA, Harrison WTA, Guloy AM: Conducting tin halides with a layered organic-based perovskite structure. Nature 1994, 369:467–469.
76 Mitzi DB, Wang S, Feild CA, Chess CA, Guloy AM: Conducting layered organic-inorganic halides containing <110>-oriented perovskite sheets. Science 1995, 267:1473–1476.
77 Feng X, Fryxell GE, Wang Q-L, Kim AY, Liu J, Kemner KM: Functionalized monolayers on ordered mesoporous supports. Science 1997, 276:923–926.
78 Weiss D, Roukes ML, Mensching A, Grambow P, Klitzing Kv, Weimann G: Electron pinball and commensurate orbits in a periodic array of scatters. Phys. Rev. Lett. 1991, 66:2790–2793.

79 Hansen W, Kotthaus JP, Merkt U: Electrons in Laterally Periodic Nanostructures, vol. 35. Ed. Hansen W, Kotthaus JP, Merkt U. San Diego:Academic Press; 1992:279–380.

80 Schechter RS, Bourrel M (Ed): Microemulsions and Related Systems: Formation, Solvency, and Physical Properties. New York: Marcel Dekker; 1988.

81 Tanford C: J. Phys. Chem. 1974, 78:2469.

82 Rosoff M (Ed): Vesicles. New York: Marcel Dekker; 1996.

83 Ringsdorf H, Schlarb B, Venzmer J: Angew. Chem., Int. Ed. Engl. 1988, 27:114–158.

84 Laughlin RG: The Aqueous Phase Behavior of Surfactants. San Diego: Academic Press; 1994.

85 Degiorgio V, Corti M (Ed): Physics of Amphiphiles: Micelles, Vesicles and Microemulsions. Amsterdam: Elsevier Science Pub. Co.; 1985.

86 Israelachvili J: Thermodynamic and geometrical aspects of amphiphile aggregation into micelles, vesicles, and bilayers, and the interactions between them. In Physics of Amphiphiles: Micelles, Vesicles and Microemulsions. Ed. Degiorgio V, Corti M; 1985:24.

87 Bates FS: Polymer–polymer phase behavior. Science 1991, 251:898–905.

88 Wennerstrom H: J. Colloid Interface Sci. 1979, 68:589–590.

89 Tiddy G: Phys. Rep. 1980, 57:1.

90 Fribreg SE, Wang J: J. Dispersion Sci. Technol. 1991, 12:387–402.

91 Walsh D, Hopwood JD, Mann S: Crystal tectonics: constructruction of reticulated calcium phosphate frameworks in bicontinuous reverse microemulsions. Science 1994, 264:1576–1578.

92 Yang JP, Qadri SB, Ratna BR: Structural and morphological characterization of pbs nanocrystallites synthesized in the bicontinuous cubic phase of a lipid. J. Phys. Chem. 1996, 100:17255–17259.

93 Braun PV, Osenar P, Stupp SI: Semiconducting superlattices templated by molecular assemblies. Nature 1996, 380:325–328.

94 Osenar P, Braun PV, Stupp SI: Adv. Mater. 1996, 8:1022.

95 Tohver V, Braun PV, Pralle MU, Stupp SI: Counterion effects in liquid crystal templating of nanostructured CdS. Chem. Mater. 1997, 9:1495–1499.

96 Braun PV, Osenar P, Tohver V, Kennedy SB, Stupp SI: Nanostructure templating in inorganic solids with organic lyotropic liquid crystals. J. Am. Chem. Soc. 1999, 121:7302–7309.

97 Attard GS, Bartlett PN, Coleman NRB, Elliott JM, Owen JR, Wang JH: Mesoporous platinum films from lyotropic liquid crystalline phases. Science 1997, 278:838–840.

98 Attard GS, Edgar M, Goltner CG: Inorganic nanostructures from lyotropic liquid crystal phases. Acta Materialia 1998, 46:751–758.

99 Elliott JM, Birkin PR, Bartlett PN, Attard GS: Platinum microelectrodes with unique high surface areas. Langmuir 1999, 15:7411–7415.

100 Attard GS, Leclerc SAA, Maniguet S, Russell AE, Nandhakumar I, Bartlett PN: Mesoporous Pt/Ru alloy from the hexagonal lyotropic liquid crystalline phase of a nonionic surfactant. Chem. Mater. 2001, 13:1444.

101 Attard GS, Leclerc SAA, Maniguet S, Russell AE, Nandhakumar I, Gollas BR, Bartlett PN: Liquid crystal phase templated mesoporous platinum alloy. Microporous Mesoporous Mater. 2001, 44:159–163.

102 Nelson PA, Elliott JM, Attard GS, Owen JR: Mesoporous nickel/nickel oxide: a nanoarchitectured electrode. Chem. Mater. 2002, 14:524–529.

103 Nandhakumar I, Elliott JM, Attard GS: Electrodeposition of nanostructured mesoporous selenium films (H-I-eSe). Chem. Mater. 2001, 13:3840.

104 Gabriel T, Nandhakumar IS, Attard GS: Electrochemical synthesis of nanostructured tellurium films. Electrochem. Commun. 2002, 4:610–612.

105 Schick MJ: Nonionic Surfactants, Physical Chemistry. New York: Marcel Dekker; 1987.

106 Wanka G, Hoffmann H, Ulbricht W: Phase diagrams and aggregation behavior of poly(oxyethylene)-poly(oxypropylene)-poly(oxyethylene) triblock copolymers in aqueous solutions. Macromolecules 1994, 27:4145–4159.

107 Fontell K: Cubic phases in surfactant and surfactant-like lipid systems. Colloid Polym. Sci. 1990, 268:264–285.

108 Lo I, Florence AT, Treguier J-P, Seiller M, Puisieux F: The influence of surfactant HLB and the nature of the oil phase on the phase diagrams of nonionic surfactant-oil-water systems. J. Colloid Interface Sci. 1977, 59:319–327.

109 Treguier JP, Seiller M, Puisieux F, Orecchioni AM, Florence AT: Effect of a hydrophilic surfactant and temperature on water-surfactant-oil diagrams. In First Expo. Cong. Int. Technol. Pharm. 1977: Assoc. Pharm.; 1977:75–87.

110 Braun PV, Stupp SI: CdS mineralization of hexagonal, lamellar, and cubic lyotropic liquid crystals. Mater. Res. Bull. 1999, 34:463–469.

111 Blackburn JC, Kilpatrick PK: Using deuterium NMR line shapes to analyze lyotropic liquid crystalline phase transitions. Langmuir 1992, 8:1679–1687.

112 Schnepp W, Disch S, Schmidt C: 2H NMR study on the lyomesophases of the system hexaethylene glycol dodecyl methyl ether/water: temperature dependence of quadrupole splittings. Liq. Cryst. 1993, 14:843–852.

113 Attard GS, Goltner CG, Corker JM, Henke S, Templer RH: Liquid-crystal templates for nanostructured metals. Angew. Chem., Int. Ed. Engl. 1997, 36:1315–1317.

114 Park M, Harrison C, Chaikin PM, Register RA, Adamson DH: Block copolymer lithography: periodic arrays of $\sim 10^{11}$ holes in one square centimeter. Science 1997, 276:1401–1404.

115 Park M, Chaikin PM, Register RA, Adamson DH: Large area dense nanoscale patterning of arbitrary surfaces. Appl. Phys. Lett. 2001, 79:257–259.

116 Li RR, Dapkus PD, Thompson ME, Jeong WG, Harrison C, Chaikin PM, Register RA, Adamson DH: Dense arrays of ordered GaAs nanostructures by selective area growth on substrates patterned by block copolymer lithography. Appl. Phys. Lett. 2000, 76:1689–1691.

117 Thurn-Albrecht T, Schotter J, Kastle CA, Emley N, Shibauchi T, Krusin-Elbaum L, Guarini K, Black CT, Tuominen MT, Russell TP: Ultrahigh-density nanowire arrays grown in self-assembled diblock copolymer templates. Science 2000, 290:2126–2129.

118 Kim HC, Jia XQ, Stafford CM, Kim DH, McCarthy TJ, Tuominen M, Hawker CJ, Russell TP: A route to nanoscopic SiO2 posts via block copolymer templates. Adv. Mater. 2001, 13:795.

119 Lin ZQ, Kim DH, Wu XD, Boosahda L, Stone D, LaRose L, Russell TP: A rapid route to arrays of nanostructures in thin films. Adv. Mater. 2002, 14:1373–1376.

120 Bal M, Ursache A, Touminen MT, Goldbach JT, Russell TP: Nanofabrication of integrated magnetoelectronic devices using patterned self-assembled copolymer templates. Appl. Phys. Lett. 2002, 81:3479–3481.

121 Shin K, Leach KA, Goldbach JT, Kim DH, Jho JY, Tuominen M, Hawker CJ, Russell TP: A simple route to metal nanodots and nanoporous metal films. Nano Lett. 2002, 2:933–936.

122 Joannopoulos JD, Meade RD, Winn JN: Photonic Crystals: Molding the Flow of Light. Princeton: Princeton University Press; 1995.

123 Busch K, John S: Photonic band gap formation in certain self-organizing systems. Phys. Rev. E 1998, 58:3896–3908.

124 Velev OD, Kaler EW: Structured porous materials via colloidal crystal templating: from inorganic oxides to metals. Adv. Mater. 2000, 12:531–534.

125 Velev OD, Jede TA, Lobo RF, Lenhoff AM: Porous silica via colloidal crystallization. Nature 1997, 389:447–448.

126 Holland BT, Blanford CF, Stein A: Synthesis of macroporous minerals with highly ordered three-dimensional arrays of spherical voids. Science 1998, 281:538–540.

127 Wijnhoven JEGJ, Vos WL: Preparation of photonic crystals made of air spheres in titania. Science 1998, 281:802–804.

128 Zakhidov AA, Baughman RH, Iqbal Z, Cui CX, Khayrullin I, Dantas SO, Marti I, Ralchenko VG: Carbon structures with three-dimensional periodicity at optical wavelengths. Science 1998, 282:897–901.

129 Mguez H, Blanco A, Meseguer F, López C, Yates HM, Pemble ME, Fornés V, Mifsud A: Brag diffraction from indium phosphide

infilled fcc silica colloidal crystals. Phys. Rev. B 1999, 59:1563–1566.
130 Blanco A, Chomski E, Grabtchak S, Ibisate M, John S, Leonard SW, Lopez C, Meseguer F, Miguez H, Mondia JP, et al.: Large-scale synthesis of a silicon photonic crystal with a complete three-dimensional bandgap near 1.5 micrometers. Nature 2000, 405:437–440.
131 Vlasov YA, Bo XZ, Sturm JC, Norris DJ: On-chip natural assembly of silicon photonic bandgap crystals. Nature 2001, 414:289–293.
132 Vlasov YA, Yao N, Norris DJ: Synthesis of photonic crystals for optical wavelengths from semiconductor quantum dots. Adv. Mater. 1999, 11:165–169.
133 Subramania G, Constant K, Biswas R, Sigalas MM, Ho K-M: Optical photonic crystals fabricated from colloidal systems. Appl. Phys. Lett 1999, 74:3933–3935.
134 Subramanian G, Manoharan VN, Thorne JD, Pine DJ: Ordered macroporous materials by colloidal assembly: a possible route to photonic bandgap materials. Adv. Mater. 1999, 11:1261–1265.
135 Mguez H, Meseguer F, López C, Holgado M, Andreasen G, Mifsud A, Fornés V: Germanium FCC structure from a colloidal crystal template. Langmuir 2000, 16:4405–4408.
136 Jiang P, Cizeron J, Bertone JF, Colvin VL: Preparation of macroporous metal films from colloidal crystals. J. Am. Chem. Soc. 1999, 121:7957–7958.
137 Braun PV, Wiltzius P: Electrochemically grown photonic crystals. Nature 1999, 402:603–604.
138 Braun PV, Zehner RW, White CA, Weldon MK, Kloc C, Patel SS, Wiltzius P: Epitaxial growth of high dielectric contrast three-dimensional photonic crystals. Adv. Mater. 2001, 13:721–724.
139 Johnson SA, Ollivier PJ, Mallouk TE: Ordered mesoporous polymers of tunable pore size from colloidal silica templates. Science 1999, 283:963–965.
140 Jeon S, Braun PV: Hydrothermal synthesis of Er-doped luminescent TiO_2 nanoparticles, Chem. Mater. 2003, 15: 1256–1263.
141 Braun PV, Wiltzius P: Electrochemical fabrication of 3-D microperiodic porous materials. Adv. Mater. 2001, 13:482–485.
142 Sumida T, Wada Y, Kitamura T, Yanagida S: Macroporous ZnO films electrochemically prepared by templating of opal films. Chem. Lett 2001, 1:38–39.
143 Pandey RK, Sahu SN, Chandra S: Handbook of Semiconductor Electrodeposition. New York: Marcel Dekker; 1996.
144 Gurunathan K, Vadivel MA, Marimuthu R, Mulik UP, Amalnerkar DP: Electrochemically synthesised conducting polymeric materials for applications towards technology in electronics, optoelectronics and energy storage devices. Mater. Chem. Phys. 1999, 61:173–191.
145 Martin CR: Nanomaterials: a membrane based synthetic approach. Science 1994, 266:1961–1966.
146 Koopal CGJ, Feiters MC, Nolte RJM, Deruiter B, Schasfoort RBM: Third generation amperometric biosensor for glucose-polypyrrole deposted within a matrix of uniform latex particles as mediator. Bioelectrochem. Bioenerg. 1992, 29:159–175.
147 Sumida T, Wada Y, Kitamura T, Yanagida S: Electrochemical preparation of macroporous polypyrrole films with regular arrays of interconnected spherical voids. Chem. Commun. 2000:1613–1614.
148 Bartlett PN, Birkin PR, Ghanem MA, Toh CS: Electrochemical syntheses of highly ordered macroporous conducting polymers grown around self-assembled colloidal templates. 2001; J. Mater. Chem. 2001, 11:849–853.
149 Cassagneau T, Caruso F: Semiconducting polymer inverse opals prepared by electropolymerization. Adv. Mater. 2002, 14:34–38.
150 Ebbesen TW, Lezec HJ, Ghaemi HF, Thio T, Wolff PA: Extraordinary optical transmission through sub-wavelength hole arrays. Nature 1998, 391:667–669.
151 Moroz A: Three-dimensional complete photonic-band-gap structures in the visible. Phys. Rev. Lett. 1999, 83:5274–5277.
152 Moroz A: Photonic crystals of coated metallic spheres. Europhys. Lett. 2000, 50:466–472.
153 Zhang WY, Lei XY, Wang ZL, Zheng DG, Tam WY, Chan CT, Sheng P: Robust photonic band gap from tunable scatterers. Phys. Rev. Lett. 2000, 84:2853–2856.

154 Oldenburg SJ, Averitt RD, Westcott SL, Halas NJ: Nanoengineering of optical resonances. Chem. Phys. Lett. 1998, 288:243–247.

155 Graf C, van Blaaderen A: Metallodielectric colloidal core-shell particles for photonic applications. Langmuir 2002, 18:524–534.

156 Wijnhoven J, Zevenhuizen SJM, Hendriks MA, Vanmaekelbergh D, Kelly JJ, Vos WL: Electrochemical assembly of ordered macropores in gold. Adv. Mater. 2000, 12:888–890.

157 Xu L, Zhou WL, Frommen C, Baughman RH, Zakhidov AA, Malkinski L, Wang JQ, Wiley JB: Electrodeposited nickel and gold nanoscale meshes with potentially interesting photonic properties. Chem. Commun. 2000:997–998.

158 Luo Q, Liu Z, Li L, Xie S, Kong J, Zhao D: Creating highly ordered metal, alloy, and semiconductor macrostructures by electrodeposition, ion spraying, and laser spraying. Adv. Mater. 2001, 13:286–289.

159 Bartlett PN, Birkin PR, Ghanem MA: Electrochemical deposition of macroporous platinum, palladium and cobalt films using polystyrene latex sphere templates. Chem. Commun. 2000:1671–1672.

160 Kokorina VF: Glasses for Infrared Optics. Boca Raton, FL: CRC Press; 1996.

161 Dunin-Borkowski RE, McCartney MR, Frankel RB, Bazylinski DA, Pósfai M, Buseck PR: Magnetic microstructure of magnetotactic bacteria by electron holography. Science 1998, 282:1868–1870.

162 Zaremba CM, Morse DE, Mann S, Hansma PK, Stucky GD: Aragonite–hydroxyapatite conversion in gastropod (abalone) nacre. Chem. Mater. 1998, 10:3813–3824.

163 Ziv V, Sabanay I, Arad T, Traub W, Weiner S: Transitional structures in lamellar bone. Microsc. Res. Technique 1996, 33:203–213.

164 Wong KKW, Douglas T, Gider S, Awschalom DD, Mann S: Biomimetic synthesis and characterization of magnetic proteins (magnetoferritin). Chem. Mater. 1998, 10:279–285.

165 Yang J, Meldrum FC, Fendler JH: Epitaxial growth of size-quantized cadmium sulfide crystals under arachidic acid monolayers. J. Phys. Chem. 1995, 99:5500–5504.

166 Rosevear, FB: Liquid Crystals: the mesomorphic phases of surfactant compositions. J. Soc. Cosmetic Chemists 1968, 19: 581–594.